NEUROSCIENCE

Microglial Calhm2 regulates neuroinflammation and contributes to Alzheimer's disease pathology

Jinbo Cheng[1,2*†], Yuan Dong[3†], Jun Ma[2], Ruiyuan Pan[2], Yajin Liao[1,2], Xiangxi Kong[2], Xiaoheng Li[2], Shuoshuo Li[2], Pingfang Chen[4], Liang Wang[5], Ye Yu[4], Zengqiang Yuan[1,2,6*]

Alzheimer's disease (AD) is the most common neurodegenerative disease in the world. Neuronal calcium dysfunction and microglial-mediated neuroinflammation are closely associated with the development of AD. However, it remains unknown whether calcium dysfunction contributes to microglial activation and, in turn, AD pathology in vivo. In this study, we demonstrated that the expression of calcium homeostasis modulator family protein 2 (Calhm2) is increased in an AD mouse model. In *5×FAD* mice carrying five familial AD gene mutations, both conventional knockout of *Calhm2* and conditional microglial knockout of *Calhm2* significantly reduced amyloid β deposition, neuroinflammation, and cognitive impairments. Mechanistically, knockout of *Calhm2* inhibited microglial proinflammatory activity but increased phagocytic activity, leading to restoration of the balance between inflammation and phagocytosis. In addition, knockout of *Calhm2* reduced acute LPS-induced neuroinflammation. These results highlight an important role for Calhm2 in microglial activation and provide a potential therapeutic target for diseases related to microglia-mediated neuroinflammation.

INTRODUCTION

Alzheimer's disease (AD), the most common neurodegenerative disease and form of dementia, is characterized by the accumulation of extracellular amyloid plaques, intracellular neurofibrillary tangles, and neuroinflammation (*1*, *2*). AD is commonly seen in aging individuals across the world; however, the molecular signaling mechanisms underlying AD pathophysiology remains unclear. This has hindered the development of effective research strategies and led to ineffective treatment options.

Recently, genome-wide association studies have shown that neuroinflammation is a genetic risk factor that mediates both the initiation and progression of AD (*3*). In human studies, more than 25 genetic loci have been associated with the risk of developing AD, and most of them are primarily expressed in microglia and linked to neuroinflammation, suggesting that microglial activation is involved in the pathophysiology of AD. Moreover, an increasing number of functional studies have demonstrated that neuroinflammation accelerates cell death and the progression of AD. These studies have uncovered and characterized the function of molecular regulators in the neuroinflammatory mechanism of AD, such as triggering receptor expressed on myeloid cells-2 (TREM2) (*4*, *5*), nucleotide-binding domain leucine-rich repeat (NLR) and pyrin domain containing receptor 3 (NLRP3) (*6*, *7*), apoptosis-associated speck-like protein containing a caspase recruitment domain (ASC) (*8*), CD33 (*9*), and CD22 (*10*). In the brain, microglia are the most abundant immune cell type, accounting for more than 80% of all immune cells (*11*). Microglia originate from the yolk sac and migrate into the central nervous system (CNS) during embryogenesis (*12*). Activated microglia are observed in multiple nervous system diseases, including AD, Parkinson's disease, and stroke. By using single-cell sorting and sequencing, a previously unknown microglia type named disease-associated microglia has been recently discovered in an AD mouse model and has been further confirmed in AD postmortem brain samples (*13*), indicating that the role of microglia in AD is more complex than previously thought. Our previous studies have demonstrated that autophagy regulates microglia-induced neuroinflammation and neurotoxicity by targeting mitochondrial antiviral signaling protein signaling and the NLRP3 inflammasome (*14*, *15*). Moreover, switching anaerobic glycolysis to mitochondrial oxidative phosphorylation could increase microglial phagocytosis and microglia-mediated amyloid β (Aβ) clearance, leading to alleviation of cognitive impairment in an AD model mouse model (*16*). Although microglia are highly associated with the progression of AD, the molecular mechanism underlying microglial activation or their phenotype switch remains largely unknown.

Calcium homeostasis is closely associated with microglial activation. For example, Aβ increases intracellular calcium levels, which, in turn, contributes to the activation of the NLRP3 inflammasome in microglia (*17*). Meanwhile, it has been demonstrated that calcium-sensing receptor activates the NLRP3 inflammasome by increasing intracellular calcium levels and decreasing cyclic adenosine 3′,5′-monophosphate levels (*18*). Moreover, the calcium channel blocker nicardipine significantly inhibits lipopolysaccharide (LPS)/interferon-γ (IFN-γ)–induced microglial activation (*19*). Recently, the role of calcium homeostasis modulator family proteins (Calhm, Calhm1, Calhm2, and Calhm3) has gained increasing attention in the field of AD research. As the most studied Calhm family member, Calhm1 controls calcium homeostasis, Aβ production, and neuronal cell vulnerability to Aβ-induced toxicity. Moreover, the P86L mutation of Calhm1 is correlated with the incidence of AD (*20*). Our previous study demonstrated that Calhm1 is expressed in human brain samples but not in mouse brain tissues and that *Calhm1* knockout mice

[1]Center on Translational Neuroscience, College of Life and Environmental Science, Minzu University of China, Beijing 100081, China. [2]The Brain Science Center, Beijing Institute of Basic Medical Sciences, Beijing 100850, China. [3]Department of Biochemistry, Medical College, Qingdao University, Qingdao, Shandong 266071, China. [4]School of Medicine, Shanghai Jiao Tong University, Shanghai 200025, China. [5]CAS Key Laboratory of Pathogenic Microbiology and Immunology, Institute of Microbiology, Center for Influenza Research and Early-warning (CASCIRE), CAS-TWAS Center of Excellence for Emerging Infectious Diseases (CEEID), Chinese Academy of Sciences, Beijing 100101, China. [6]Center of Alzheimer's Disease, Beijing Institute for Brain Disorders, Beijing 100069, China.
*Corresponding author. Email: cheng_jinbo@126.com (J.C.); zqyuan@bmi.ac.cn or zyuan620@yahoo.com (Z.Y.)
†These authors contributed equally to this work as co-first authors.

show no significant cognitive deficits (*21*). However, another study showed that Calhm1, expressed specifically in type II taste bud cells, functions as a voltage-gated adenosine 5′-triphosphate (ATP) release channel in regulating taste perception (*22*). Subsequent studies showed that Calhm3 interacts with Calhm1 and that the deletion of *Calhm3* abolished taste-evoked ATP release (*23*). Accordingly, we found that Calhm2, which is highly expressed in the murine brain, could regulate ATP release in astrocytes and that *Calhm2* deletion induced a depression-like phenotype in mice (*24*). Among the Calhm family members, only Calhm2 is abundantly expressed in the CNS; however, its role in the nervous system is still largely unknown, especially in AD-related processes.

In this study, we found that the levels of Calhm2 significantly increased in AD mouse models. Conventional knockout of *Calhm2* and microglial-specific knockout of *Calhm2* both significantly decreased Aβ deposition, neuroinflammation, and alleviated AD-related cognitive impairments. Mechanistically, we found that Calhm2 regulates calcium influx and inflammatory activation in microglia, implicating a potential therapeutic target for AD.

RESULTS

Calhm2 levels are increased in patients with AD and in AD mice

To assess the involvement of Calhm family members in AD, we analyzed expression changes using the AlzData web server (www.alzdata.org). In the GSE48350 dataset, human *Calhm2* and *Calhm3* were significantly increased in hippocampal tissue samples of patients with AD compared to the control group, with no change in *Calhm1* (Fig. 1A). In the GSE5281 dataset, only *Calhm2* levels increased in the hippocampal tissue samples of patients with AD, shown in Fig. 1B. Moreover, we have used quantitative polymerase chain reaction (qPCR) method to validate the levels of *Calhm2* mRNA in the hippocampal tissue samples of patients with AD and found that *Calhm2* mRNA levels increased in patients with AD (fig. S1A). These results suggest that Calhm2 might be involved in the development of AD. To further confirm this, we analyzed *Calhm2* levels in 6-month-old *5×FAD* model mice, a commonly used AD mouse model that expresses five familial AD gene mutations, and found a significant increase in *Calhm2* levels within the hippocampus of the AD mice (Fig. 1C).

To characterize the expression pattern of Calhm2 in the brain, we used fluorescent RNAscope probes, a sensitive in situ hybridization (ISH) technique, and found that *Calhm2* is highly expressed in the cortex and hippocampus in the mouse brain, with low levels in the striatum. Meanwhile, expression of *Calhm2* was not observed in brain sections of *Calhm2* knockout mice (fig. S2, A to C). Furthermore, to study the cellular expression pattern of *Calhm2*, we used an ISH-immunofluorescence method [i.e., performed the ISH of Calhm2 first and then performed immunofluorescence staining for ionized calcium-binding adaptor molecule 1 (Iba1) or glial fibrillary acidic protein (GFAP)] in which *Calhm2* signal can be easily detected in microglia and astrocytes (fig. S2D). Moreover, we stained *Calhm2* with *NeuN* (neuron marker), *Gfap* (astrocyte marker), or *Cx3cr1* (microglia marker) and found that *Calhm2* signal was detected in neurons, astrocytes, and microglia, and the *Calhm2* spot number per cell was higher in microglia compared with astrocyte and neurons (Fig. 1, D and E). Furthermore, we found that *Calhm2* levels were increased in activated microglia (characterized by decreased process length and increased soma area) in 6-month-old AD mice, with no significant changes in astrocyte (Fig. 1, F and G). Together, these results indicated that *Calhm2* is increased in the AD brain, suggesting that Calhm2 might have an important role in the pathophysiology of AD.

Calhm2 knockout restores cognitive functions, decreases Aβ deposition, and decreases glial numbers in *5×FAD* mice

To assess the role of Calhm2 in the development of AD, we used a *Calhm2* knockout mouse line and crossed with a *5×FAD* mouse (Fig. 2A). Levels of Calhm2 were assessed in all four groups [wild-type (WT) mice, $Calhm2^{-/-}$ mice, *5×FAD* mice, and $Calhm2^{-/-}$:*5×FAD* mice] of mice at 5 months old. As shown in Fig. 2B, the levels of Calhm2 were increased in WT AD mice and were undetectable in *Calhm2* knockout mice. Next, we checked whether *Calhm2* knockout affected the learning and memory impairment using the Morris water maze (MWM) task. As shown in Fig. 2C, AD mice spent more time reaching the platform in the training period, suggesting the presence of a cognitive deficit. Notably, knockout of *Calhm2* significantly improved task learning. Consistently, during the test period, knockout of *Calhm2* resulted in significantly decreased time to reach the platform, increased preference for the target quarter, and increased number of platform crossings but no significant alteration in swimming speed (Fig. 2, D to H); this suggested alleviation of the cognitive impairment.

Next, we checked whether knockout of *Calhm2* altered Aβ levels within the brain. As shown in Fig. 2 (I and J), *Calhm2* knockout markedly decreased Aβ plaques within the cortex and hippocampus. We then quantified the concentration of Aβ species by enzyme-linked immunosorbent assay (ELISA). Notably, there were significant reductions in soluble $Aβ_{1–42}$, insoluble $Aβ_{1–42}$, and insoluble $Aβ_{1–40}$ levels, with a decreased trend of soluble $Aβ_{1–40}$ levels (Fig. 2, K to N), suggesting that *Calhm2* knockout decreased the deposition of total Aβ in the brain. Furthermore, we found that *Calhm2* knockout failed to affect the levels of key regulators of amyloid precursor protein (APP) metabolism, such as APP, β site APP cleaving enzyme, nicastrin, and presenilin 2 (fig. S3, A and B), suggesting that *Calhm2* knockout did not influence APP metabolism. To further confirm this, we used a $Calhm2^{flox/flox}$ mouse line and crossed it with a *CamKIIα-iCre* mouse to get a conditional neuronal *Calhm2* knockout mouse line. We then crossed this mouse with a *5×FAD* mouse (fig. S3C). At 6 months old, we found that Calhm2 levels significantly decreased in the $Calhm2^{flox/flox:\ CamKIIa\text{-}iCre}$:*5×FAD* mouse; however, the key regulators involved in APP metabolism were not significantly changed (fig. S3, D to F). In addition, neither soluble or insoluble $Aβ_{1–40}$ and $Aβ_{1–42}$ levels were significantly changed, relative to the $Calhm2^{flox/flox}$:*5×FAD* mice (fig. S3, G to J), suggesting that neuronal Calhm2 may not be involved in the production and the deposition of Aβ.

Neuroinflammation is always present in AD and serves as a key regulator for the development of AD (*25*). We thus checked the effect of *Calhm2* knockout on the glial numbers. As shown in Fig. 2 (O to R), knockout of *Calhm2* significantly decreased the numbers of microglia and astrocytes within the cortex and hippocampus. The protein levels of Iba1 and GFAP were also consistently significantly reduced in *Calhm2* knockout AD mice (fig. S3, K to M). Together, these results suggest that knockout of *Calhm2* significantly decreased both Aβ deposition and neuroinflammation.

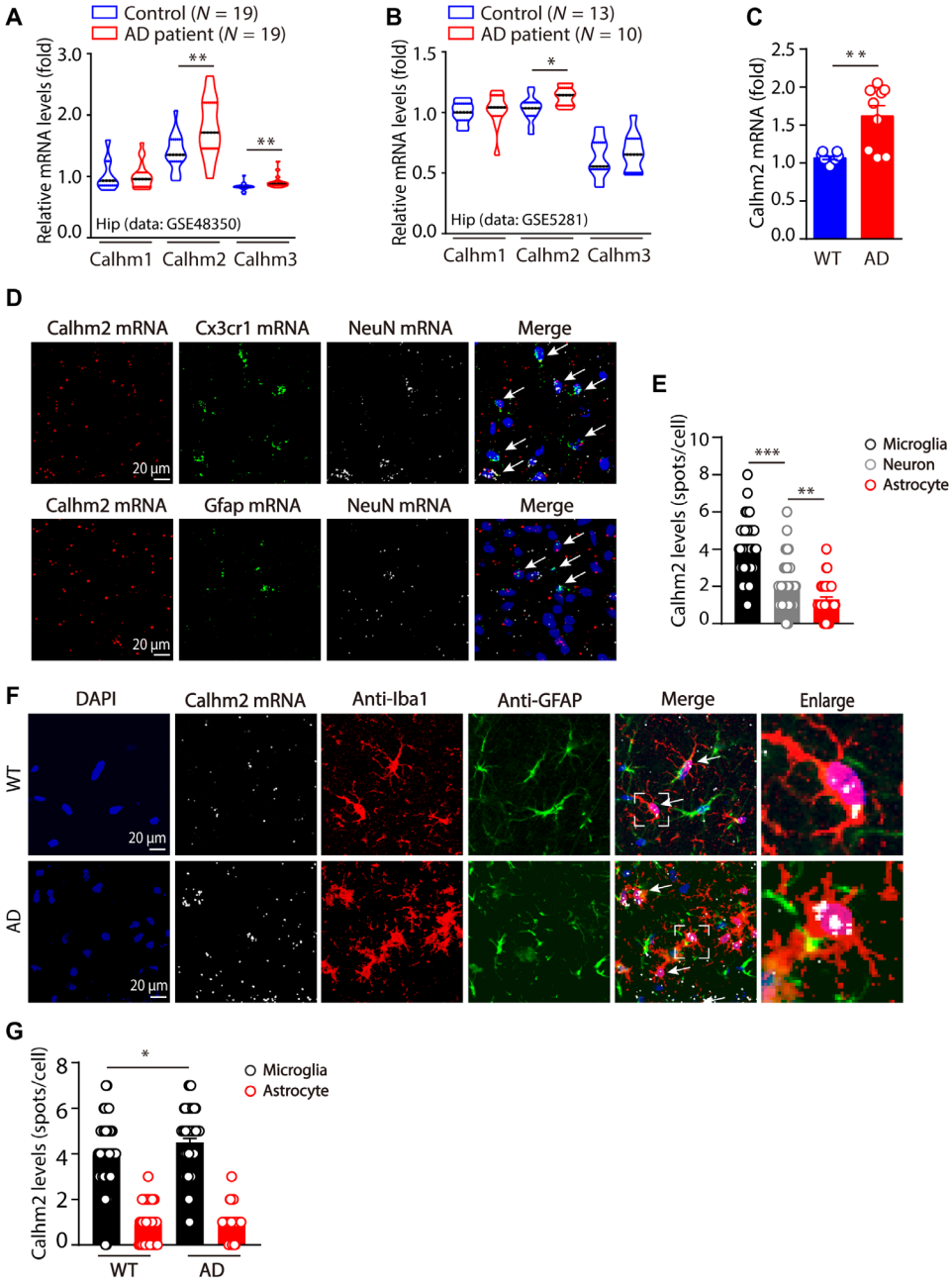

Fig. 1. Calhm2 levels are increased in patients with AD and in AD mice. (**A** and **B**) Transcriptional up-regulation of *Calhm2* in hippocampal (Hip) tissue of patients with AD in the GSE48350 database (control, $n = 19$; AD patient, $n = 19$) and GSE5281 database (control, $n = 13$; AD patient, $n = 10$). (**C**) Transcriptional up-regulation of *Calhm2* in the hippocampus of 6-month-old *5×FAD* mice (WT mice, $n = 9$; AD mice, $n = 9$). (**D** and **E**) Coexpression and quantification of *Calhm2* mRNA [in situ hybridization (ISH)] and *Cx3cr1* mRNA (ISH), Gfap mRNA (ISH), and *NeuN* mRNA (ISH) in the hippocampus of 6-month-old WT mice. (**F**) RNA ISH of *Calhm2* expression and its colocalization with Iba1 (immunostaining)– and GFAP (immunostaining)–positive cells in 6-month-old WT and *5×FAD* mice. (**G**) The quantification of Calhm2 levels in microglia and astrocytes from 6-month-old WT and *5×FAD* mice. $^{*}P < 0.05$, $^{**}P < 0.01$, and $^{***}P < 0.001$.

Microglial *Calhm2* knockout restores cognitive functioning and decreases Aβ deposition

We next asked in which cell type Calhm2 functions in the development of AD. Given that Calhm2 was expressed in microglia and increased in activated microglia and that microglia play a key role in Aβ clearance and neuroinflammation, we used a microglial-specific knockout of *Calhm2* mouse line using a $Cx3cr1^{CreER}$ mouse (*26*) and then crossed it with a *5×FAD* mouse. To exclude the effects of Calhm2 in peripheral macrophages, we injected tamoxifen at postnatal day 45 and performed the behavioral tests at 5 months old and pathological analysis at 6 months old, as peripheral macrophages confer a rapid turnover and are replenished in 1 month (Fig. 3A). At 5 months old, we isolated microglia from the brain and confirmed a high *Calhm2* knockout efficiency (Fig. 3B). Furthermore, we performed a visible platform task and found that microglial *Calhm2* knockout failed to influence the latency to the platform and

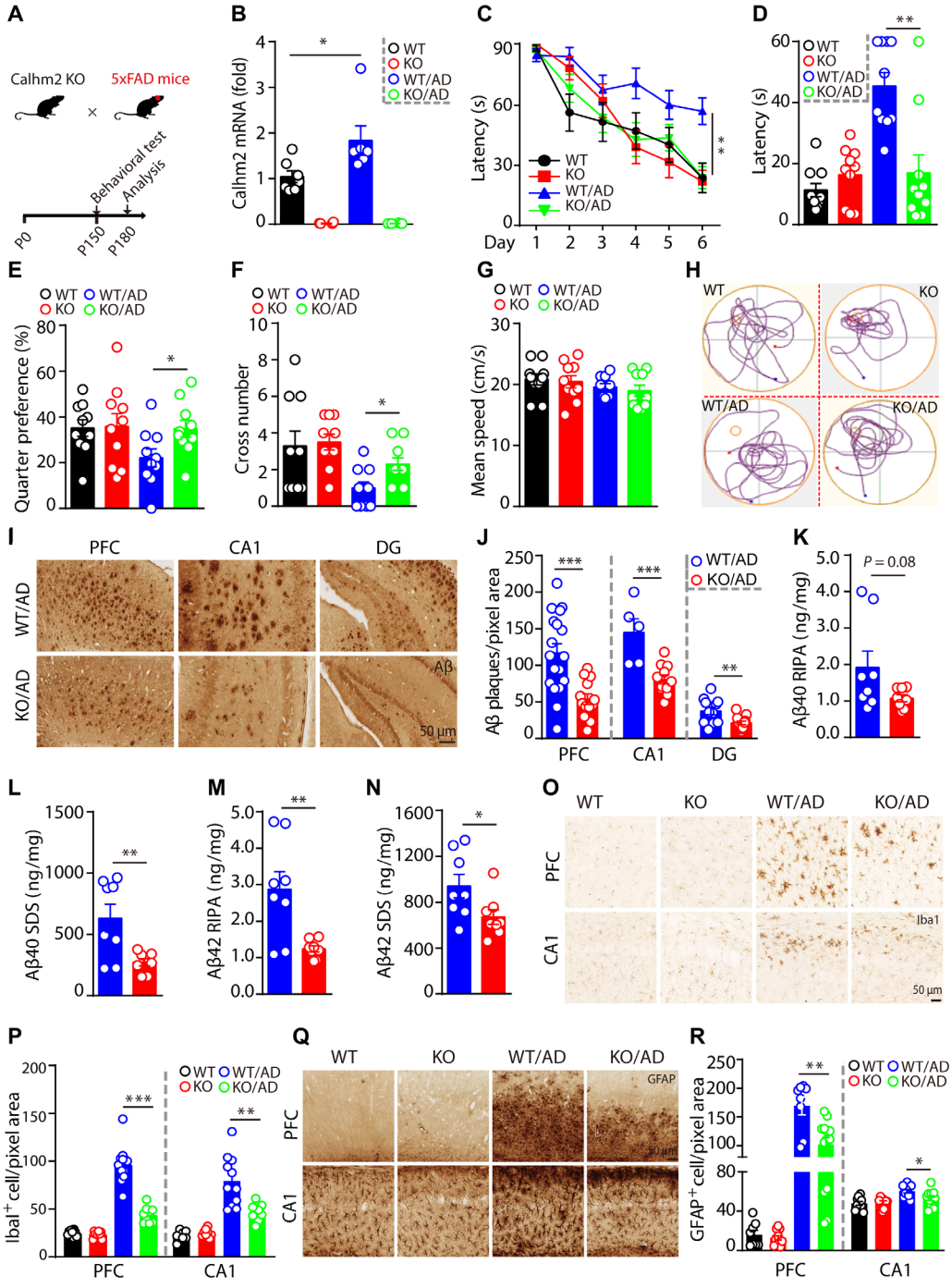

Fig. 2. *Calhm2* knockout restores cognitive functions, decreases Aβ deposition, and decreases glial numbers in *5×FAD* mice. (**A**) Schematic for the generation of *Calhm2*$^{-/-}$*:5×FAD* mice, behavioral tests, and pathological analysis. KO, knockout. (**B**) Transcriptional levels of Calhm2 in the hippocampus of 6-month-old WT ($n = 7$), *Calhm2*$^{-/-}$ ($n = 6$), *5×FAD* ($n = 6$), and *Calhm2*$^{-/-}$*:5×FAD* mice ($n = 10$). (**C**) MWM analysis as latency (s) to target in the invisible platform trainings. (**D** to **G**) MWM analysis as the latency (s), target quarter preference (%), target cross number, and mean speed (cm/s) in the invisible platform tests in 5-month-old WT ($n = 10$ mice), *Calhm2*$^{-/-}$ ($n = 10$ mice), *5×FAD* ($n = 10$ mice), and *Calhm2*$^{-/-}$*:5×FAD* mice ($n = 10$ mice). (**H**) Representative images of the track plots in the MWM tests. (**I** and **J**) Immunohistochemistry (IHC) and statistical analysis of Aβ plaques per pixel area in the prefrontal cortex (PFC) ($n = 13$ to 18 slices from three mice per group), CA1 ($n = 6$ to 11 slices from three mice per group), and dentate gyrus (DG) ($n = 11$ to 13 slices from three mice per group) of *5×FAD* and *Calhm2*$^{-/-}$*:5×FAD* mice. (**K** to **N**) ELISA method for detecting soluble [radioimmunoprecipitation assay (RIPA) fraction] and insoluble (SDS fraction) contents of $A\beta_{1-40}$ and $A\beta_{1-42}$ of *5×FAD* and *Calhm2*$^{-/-}$*:5×FAD* mice ($n = 8$ per group). (**O** and **P**) IHC and statistical analysis of Iba1-positive cells (microglia) per pixel area in 6-month-old WT, *Calhm2*$^{-/-}$ mice, *5×FAD*, and *Calhm2*$^{-/-}$*:5×FAD* mice. (**Q** and **R**) IHC and statistical analysis of GFAP-positive cells (astrocytes) per pixel area in 6-month-old WT mice, *Calhm2*$^{-/-}$ mice, *5×FAD* mice, and *Calhm2*$^{-/-}$*:5×FAD* mice ($n = 8$ to 13 slices from three mice per group). Scale bar, 50 μm. One-way analysis of variance (ANOVA) for multiple groups in (C) to (G) were based on mouse number. Statistical analysis of (I), (O), (P), (Q), and (R) were dependent on multiple sampling. *$P < 0.05$, **$P < 0.01$, and ***$P < 0.001$.

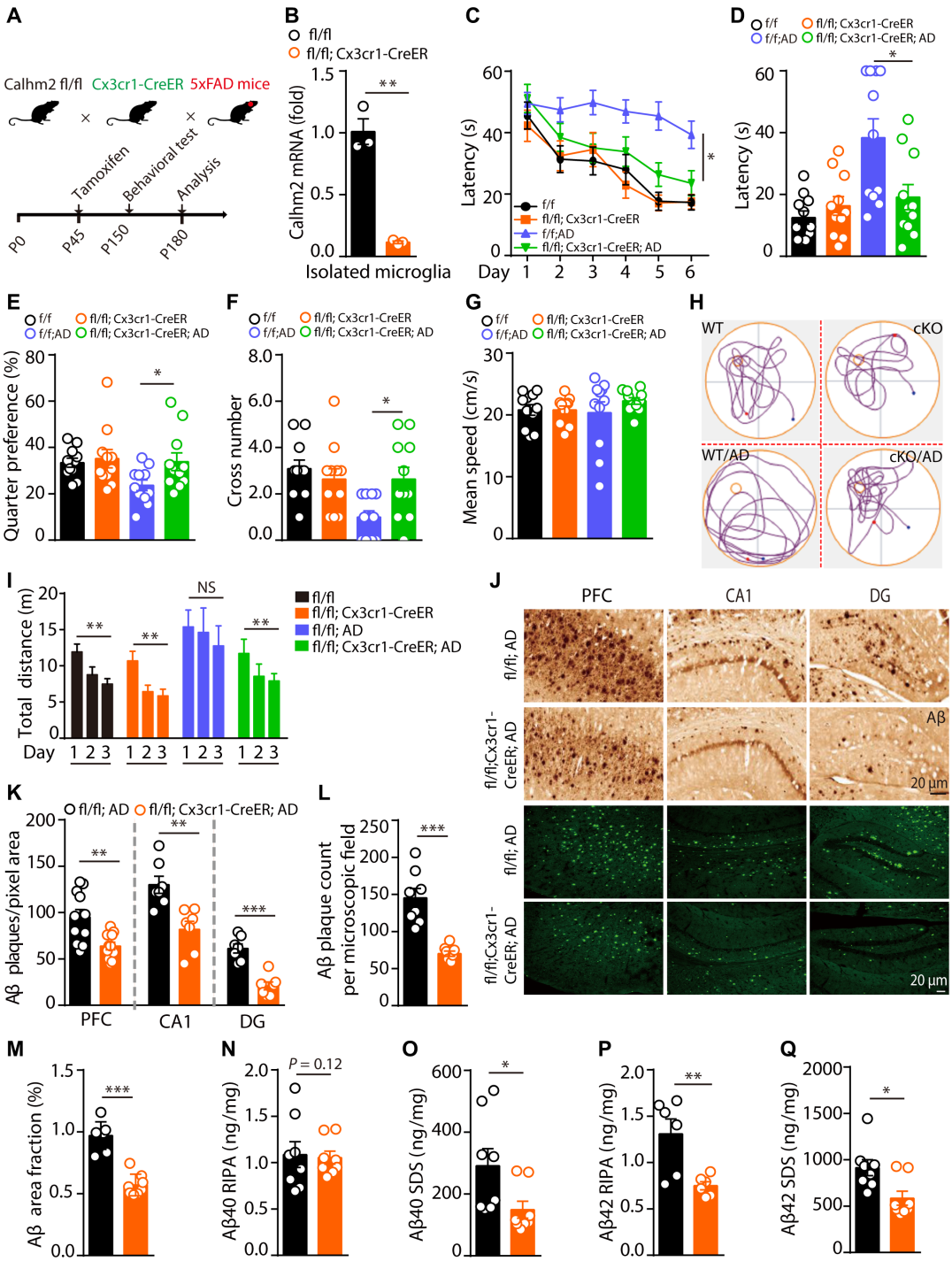

Fig. 3. Microglial *Calhm2* knockout restores cognitive function and decreases amyloid beta deposition in *5×FAD* mice. (**A**) Schematic for the generation of *Calhm2*$^{flox/flox:Cx3cr1\text{-}CreER}$*:5×FAD* mice, intragastric tamoxifen administration, behavioral testing, and pathological analysis. P0, postnatal day 0. (**B**) Transcriptional levels of Calhm2 in isolated microglia of 5-month-old *Calhm2*$^{flox/flox}$ and *Calhm2*$^{flox/flox:Cx3cr1\text{-}CreER}$ mice ($n = 3$ mice). (**C**) MWM analysis as latency (s) to target in the invisible platform trainings. (**D** to **G**) MWM analysis as the latency (s), target quarter preference (%), target cross number, and mean speed (centimeters per second) in the invisible platform tests in 5-month-old *Calhm2*$^{flox/flox}$ ($n = 11$ mice), *Calhm2*$^{flox/flox:Cx3cr1\text{-}CreER}$ ($n = 11$ mice), *Calhm2*$^{flox/flox}$*:5×FAD* ($n = 11$ mice), and *Calhm2*$^{flox/flox:Cx3cr1\text{-}CreER}$*:5×FAD* ($n = 11$ mice) mice. (**H**) Representative images of track plots in the MWM tests. cKO, conditional knockout. (**I**) Open-field test and locomotor activity (distance traveled) over three consecutive days. (**J** and **K**) IHC and immunofluorescent staining and statistical analysis of Aβ plaques per pixel area in the PFC, CA1, and DG of *Calhm2*$^{flox/flox}$*:5×FAD* and *Calhm2*$^{flox/flox:Cx3cr1\text{-}CreER}$*:5×FAD* mice ($n = 7$ to 11 slices from three mice per group). (**L** and **M**) Statistical analysis of thioflavin S staining (compact Aβ plaque) of Aβ plaques in the PFC of *Calhm2*$^{flox/flox}$*:5×FAD* and *Calhm2*$^{flox/flox:Cx3cr1\text{-}CreER}$*:5×FAD* mice ($n = 8$ slices from three mice per group). (**N** to **Q**) ELISA analysis of soluble (RIPA fraction) and insoluble (SDS fraction) contents of $A\beta_{1-40}$ and $A\beta_{1-42}$ of *Calhm2*$^{flox/flox}$*:5×FAD* and *Calhm2*$^{flox/flox:Cx3cr1\text{-}CreER}$*:5×FAD* mice ($n = 8$ per group). One-way ANOVA for multiple groups in (C) to (G) and (I) were based on mouse number. Statistical analysis of (J) to (M) were dependent on multiple sampling. NS, no significance; $^*P < 0.05$, $^{**}P < 0.01$, and $^{***}P < 0.001$.

the distance traveled (fig. S4, A to C), suggesting that microglial *Calhm2* knockout had no effect on vision and swimming ability. Notably, using the invisible platform MWM test, we found that microglial *Calhm2* knockout significantly decreased the latency to the platform and increased the target quarter preference and the crossing numbers, with no significant difference in swimming speed (Fig. 3, C to H), suggesting that microglial *Calhm2* knockout alleviates cognitive impairment in AD mice. To test whether microglial *Calhm2* knockout had any influences on emotion, we performed the open-field test and found that center entries and the time spent in center were not significant different among these four groups of mice on day 1 of testing (fig. S4, D and E). However, after 3 days of consecutive testing, microglial *Calhm2* knockout significantly decreased the total distance moved (Fig. 3I), suggesting a reduction in locomotion and habituation to the task. Together, these results suggest a detrimental role of microglial Calhm2 in the behavioral and cognitive dysfunction in the development of AD.

Next, we found that microglial *Calhm2* knockout had no effect on APP metabolism (fig. S5, A and B) but markedly reduced Aβ plaques within the cortex and hippocampus (Fig. 3, J and K). Consistently, thioflavin S staining also showed a significant reduction, suggesting a decrease in Aβ levels within the brain (Fig. 3, J, L, and M). Furthermore, using ELISA method, we found that the soluble and insoluble $A\beta_{1-42}$ were significantly decreased in microglial *Calhm2* knockout mice. The insoluble $A\beta_{1-40}$ was also significantly reduced, with a decreasing trend of soluble $A\beta_{1-40}$ levels (Fig. 3, N to Q). Together, these results demonstrated that microglial *Calhm2* knockout decreased the Aβ levels and alleviated behavioral as well as cognitive dysfunction in AD mice.

Microglial *Calhm2* knockout increases phagocytotic activity in microglia

To investigate the role of microglial *Calhm2* knockout in neuroinflammation, we analyzed glial numbers and found that there was the lower amount of reactive microglia and astrocytes within the cortex and hippocampus in microglial *Calhm2* knockout AD mice (Fig. 4, A to C). Consistently, the protein levels of Iba1 and GFAP were also significantly decreased (Fig. 4, D and E). We then quantified the mRNA levels of the microglia marker CD11b, the astrocyte marker GFAP, and various inflammatory cytokines, which revealed that the levels of CD11b and GFAP were significantly inhibited in microglial *Calhm2* knockout AD mice. In addition, levels of the proinflammatory cytokine interleukin-1β (IL-1β), which is reported to suppress microglial clearance activity (*6*, *27*), were also largely decreased. Levels of anti-inflammatory Arg1 were increased, with no significant difference in inducible nitric oxide synthase, IL-6, and CD206 (fig. S5C). Next, we analyzed the effect of Calhm2 on microglial phagocytic activity. We found that microglial *Calhm2* knockout significantly increased the numbers of microglia around Aβ plaques (Fig. 4, F and G), suggesting increased activity of microglial phagocytosis. In addition, we quantified the levels of CD68, a lysosome marker indicating the degradative activity of microglia (*28*), and found that the density of CD68 was significantly increased in the *Calhm2* knockout microglia, suggesting higher degradation activity (Fig. 4, H and I). TREM2 is a phagocytic receptor that is mainly expressed in microglia and has a critical role in AD (*29*). The mutation R47H in TREM2 that leads to loss of ligand binding ability has been linked to the risk of AD (*30*). *TREM2* deficiency impairs microglial metabolic fitness and Aβ degradation (*4*, *5*). We found that microglial *Calhm2* knockout increased TREM2 immunostaining signals around Aβ plaques in the AD mouse brain (Fig. 4, J and K). Consistently, the numbers of Aβ plaque sizes were decreased in microglial *Calhm2* knockout mice brain (fig. S5D). To further confirm this, we isolated primary microglia and studied the effect of *Calhm2* knockout on microglial phagocytosis of Aβ in vitro. We found that *Calhm2* knockout increased TREM2 levels in vitro (Fig. 4L and fig. S5E). In addition, after 1 and 3 hours of aggregated Aβ incubation, there were higher levels of Aβ in the *Calhm2* knockout microglia, with lower levels in the culture medium (Fig. 4M and fig. S5, F and G). Consistently, by using fluorescein isothiocyanate (FITC)–labeled Aβ, we also observed more FITC-Aβ in *Calhm2* knockout microglia (fig. S5, H and I), suggesting an increased phagocytic ability. Together, these in vivo and in vitro results demonstrated that microglial *Calhm2* knockout suppressed inflammatory levels and increased the phagocytosis of Aβ.

The microglial transcriptome analysis revealed a protective role of *Calhm2* knockout in *5×FAD* mice

To further investigate the molecular mechanisms underlying the functions of Calhm2 in AD, we isolated primary microglia from these four groups of mice ($Calhm2^{flox/flox}$ mice, $Calhm2^{flox/flox:Cx3cr1\text{-}CreER}$ mice, $Calhm2^{flox/flox}$:*5×FAD* mice, and $Calhm2^{flox/flox:Cx3cr1\text{-}CreER}$:*5×FAD* mice) and performed RNA sequencing (RNA-seq) analysis (Fig. 5A). We identified 1109 up-regulated genes and 1240 down-regulated genes in the microglia of AD groups, compared to the WT groups. Notably, microglial *Calhm2* knockout restored the levels of most of the up-regulated genes and increased the levels of many of the down-regulated genes (Fig. 5B), which is consistent with the rescue phenotype of microglia numbers and inflammatory cytokine levels. Then, we performed the principal components analysis and gene ontology (GO) analysis of the significantly changed genes in *Calhm2* conditional knockout microglia, and WT microglia revealed a significant functional reduction in cell migration and cell proliferation in AD mice. In addition, immune response (including response to oxidative stress and response to LPS), immune signaling, cell surface, vesicle, ion transport, and channel activity were significantly down-regulated in *Calhm2* knockout microglia (fig. S6, A and B). Meanwhile, proteolysis activity, protein ubiquitination, DNA repair, neurogenesis, cognition, and learning/memory-related signaling were increased and enriched, suggesting a protective role of Calhm2 deficiency in microglia-induced neurotoxicity (fig. S6C). Next, we performed gene set enrichment analyses (GSEAs) and found that G2M checkpoint genes were highly enriched in *Calhm2* conditional knockout microglia in AD mice, suggesting an inhibition of microglial proliferation (fig. S6D). In addition, the unfolded protein response gene set was increased, but the IFN-α response, IFN-γ response, reactive oxygen species (ROS) pathway, tumor necrosis factor–α (TNFα) signaling via nuclear factor κB (NF-κB), and IL-6/Janus kinase (JAK)/signal transducer and activator of transcription 3 (Stat3) signaling were significantly down-regulated (Fig. 5, C and D, and fig. S6, E to H), suggesting an inhibition of inflammatory activation.

To further characterize the inflammatory changes, we analyzed the levels of microglial homeostasis genes, innate immunity signaling genes, complement signaling genes, and inflammatory cytokines. As shown in Fig. 5E, microglial markers Aif (Iba1) and Itgam (CD11b) were not significantly changed in microglia in AD, and knockout of *Calhm2* also did not influence their expression levels. Deletion of *Calhm2* significantly reduced the increases of complement

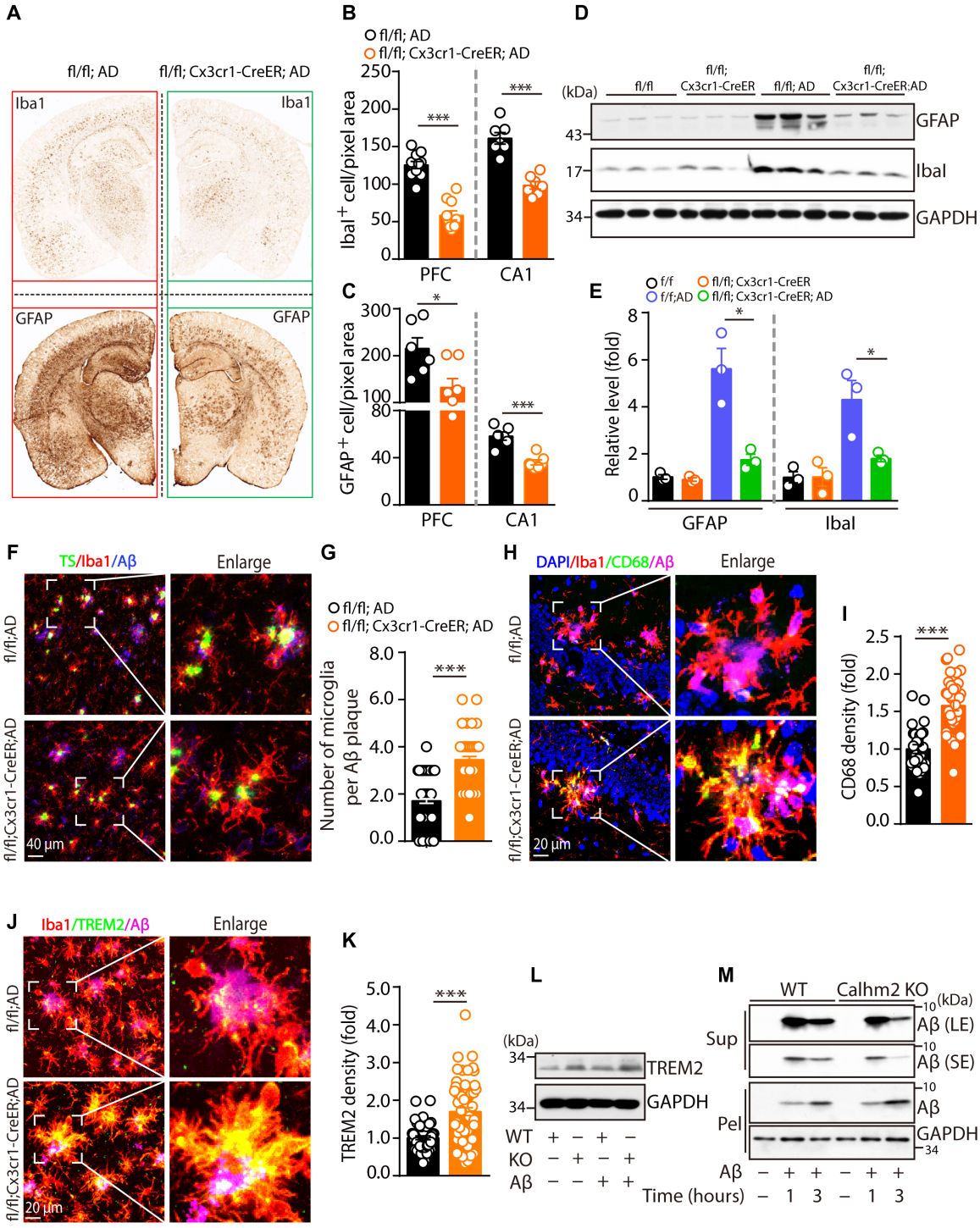

Fig. 4. Microglial *Calhm2* knockout increases microglial phagocytosis activation. (**A** to **C**) IHC and statistical analysis of Iba1- and GFAP-positive cells in PFC and CA1 of 6-month-old *Calhm2*$^{flox/flox}$:*5×FAD* and *Calhm2*$^{flox/flox:Cx3cr1\text{-}CreER}$:*5×FAD* mice ($n = 7$ to 11 slices from three mice per group). (**D** and **E**) Immunoblotting and statistical analysis of Iba1 and GFAP levels of 6-month-old *Calhm2*$^{flox/flox}$, *Calhm2*$^{flox/flox:Cx3cr1\text{-}CreER}$, *Calhm2*$^{flox/flox}$:*5×FAD*, and *Calhm2*$^{flox/flox:Cx3cr1\text{-}CreER}$:*5×FAD* mice ($n = 3$ per group). (**F** and **G**) Thioflavin S staining, immunofluorescent staining of Iba1 and Aβ, and statistical analysis of microglia number per Aβ plaque of 6-month-old *Calhm2*$^{flox/flox}$:*5×FAD* and *Calhm2*$^{flox/flox:Cx3cr1\text{-}CreER}$:*5×FAD* mice ($n > 50$ from three mice per group). (**H** and **I**) Immunofluorescent staining of Iba1, CD68, and Aβ and statistical analysis of CD68 density of 6-month-old *Calhm2*$^{flox/flox}$:*5×FAD* and *Calhm2*$^{flox/flox:Cx3cr1\text{-}CreER}$:*5×FAD* mice ($n > 25$ from three mice per group). (**J** and **K**) Immunofluorescent staining of Iba1, TREM2, and Aβ and statistical analysis of TREM2 density of 6-month-old *Calhm2*$^{flox/flox}$:*5×FAD* and *Calhm2*$^{flox/flox:Cx3cr1\text{-}CreER}$:*5×FAD* mice ($n > 50$ from three mice per group). (**L**) Immunoblotting TREM2 levels in primary microglia of WT and *Calhm2*$^{-/-}$ with and without Aβ (1 μg/ml, 3 hours) treatment. (**M**) Immunoblotting of Aβ levels of WT and *Calhm2*$^{-/-}$ in the supernatant (Sup) and pellet (Pel) of primary microglia. Statistical analysis of (B), (C), and (F) to (K) were dependent on multiple sampling. *$P < 0.05$ and ***$P < 0.001$. SE, short exposure; LE, long exposure.

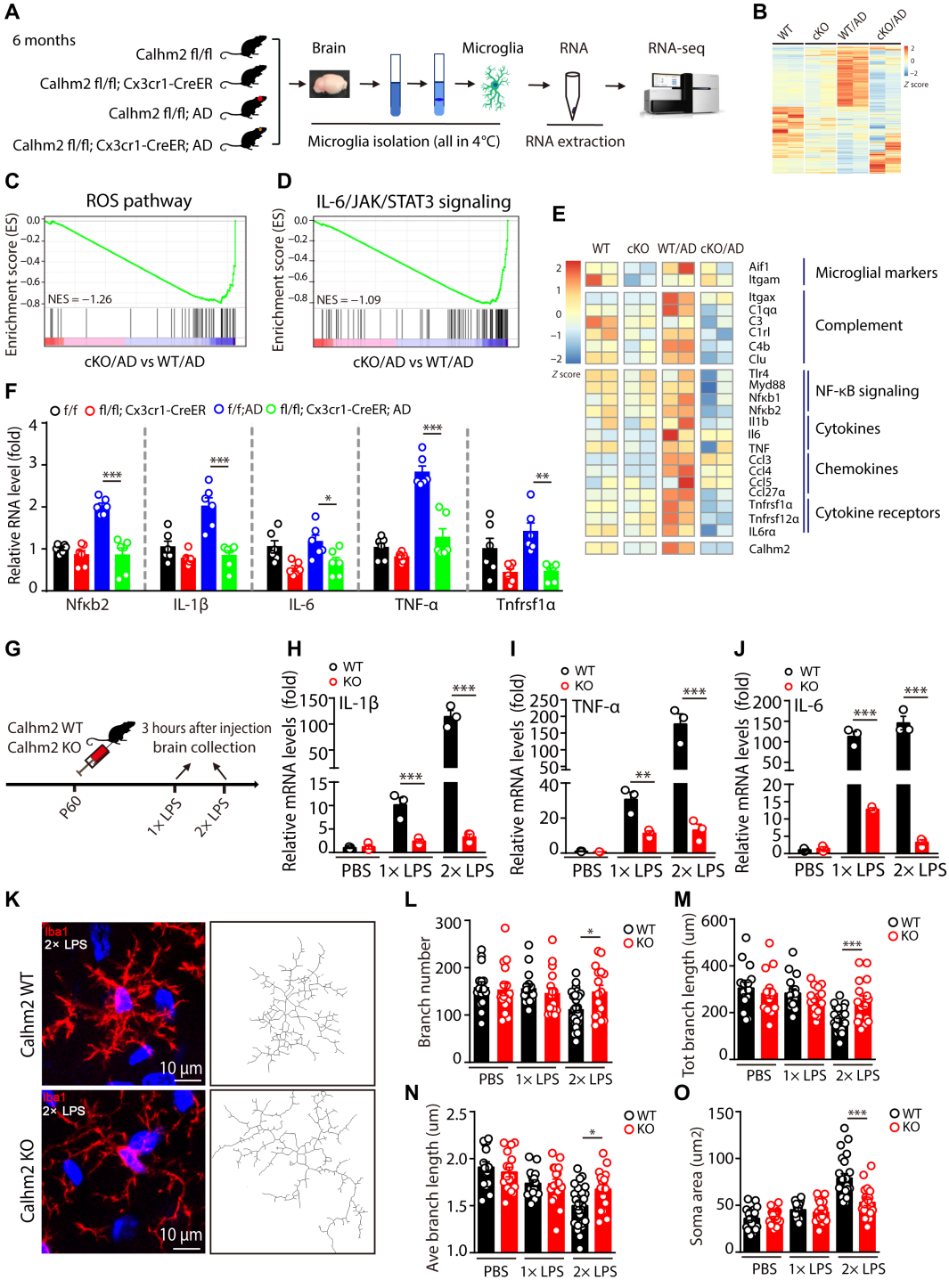

Fig. 5. Microglial transcriptome changes reveal a protective role for *Calhm2* knockout in *5×FAD* mice. (**A**) Schematic for microglia isolation, RNA extraction, RNA-seq, and bioinformatic analysis. (**B**) Heatmap shows four groups of expressed genes that differentially expressed between 6-month-old *Calhm2*$^{flox/flox}$ mice and *Calhm2*$^{flox/flox}$*:5×FAD* mice (log_2 fold change > 0.5, adjusted false discovery rate < 0.05). (**C** and **D**) GSEA of the ROS pathway and IL-6/JAK/Stat3 signaling of 6-month-old *Calhm2*$^{flox/flox:Cx3cr1\text{-}CreER}$*:5×FAD* versus *Calhm2*$^{flox/flox}$*:5×FAD*. GAPDH, glyceraldehyde-3-phosphate dehydrogenase. (**E**) Heatmap of microglial markers, complement, NF-κB signaling, cytokines, chemokines, and cytokines receptors in microglia from these four groups of mice. (**F**) qPCR assay to test the expression levels of indicated genes in isolated microglial cells from these four groups mice ($n = 6$ per group). (**G**) Schematic for intraperitoneal LPS injections in 2-month-old WT and *Calhm2*$^{-/-}$ mice. (**H** to **J**) Transcriptional levels of IL-1β, TNF-α, and IL-6 in 2-month-old WT and *Calhm2*$^{-/-}$ mice after intraperitoneal LPS injections ($n = 3$ mice per group). (**K**) Immunofluorescence staining of Iba1-positive cells within the hippocampus of WT and *Calhm2*$^{-/-}$ mice. (**L** to **O**) Skeletonized analysis: Representative images and statistical analysis of branch numbers, total branch length (micrometers), average branch length (micrometers), and soma area (square micrometers) of Iba1-positive cells within the hippocampus of WT and *Calhm2*$^{-/-}$ mice ($n > 20$ from three mice per group). Statistical analysis of (L) to (O) were dependent on multiple sampling. *$P < 0.05$, **$P < 0.01$, and ***$P < 0.001$.

genes (Itgax, C1qa, C1rl, C4b, and Clu), NF-κB signaling genes (Tlr4, Myd88, Nfkb1, and Nfkb2), cytokines (IL-1β, TNFα, and IL-6), chemokines (Ccl3, Ccl4, Ccl5, and Ccl27a), and some cytokines receptors (Tnfrsf1a, Tnfrsf12a, and IL6r1a), which are consistent with the down-regulation of the immune response. Furthermore, we performed qPCR assay to validate the changes in isolated microglia. As shown in Fig. 5F, knockout of *Calhm2* significantly decreased the NF-κB signaling gene Nfkb2, cytokines (IL-1β, IL-6, and TNFα), and the cytokines receptor Tnfrsf1a in the isolated microglia from AD mice. Together, these results suggested an inhibitory effect of *Calhm2* knockout on the immune response in AD microglial cells.

Calhm2 knockout inhibits LPS-induced neuroinflammation in vivo and in vitro

To further investigate the role of Calhm2 in neuroinflammation, we established an acute LPS injection mouse model as previously described (*31*). Intraperitoneal injection of LPS significantly increased the level of some inflammatory cytokines, including IL-1β, TNFα, and IL-6. Notably, knockout of *Calhm2* markedly inhibited the level of these cytokines (Fig. 5, G to J), suggesting a vital role for Calhm2 in mediating neuroinflammation. Furthermore, we analyzed the changes in microglial morphology by staining Iba1. Two LPS injections induced significant changes to the microglial morphology, characterized by decreased branch numbers, total branch length, and average branch length, and a significant increase in soma area. *Calhm2* knockout significantly rescued LPS-induced morphological changes (Fig. 5, K to O). To specifically study the role of Calhm2 in microglia, we used a conditional microglial *Calhm2* knockout mouse line and performed the same acute LPS injection treatment. We found that levels of the cytokines IL-1β, TNFα, and IL-6 were also significantly inhibited in the microglial *Calhm2* knockout mice (fig. S7, A to D). In addition, microglial *Calhm2* knockout rescued most of the microglial morphological changes induced by LPS injection (fig. S7, E to J). We found that both conventional knockout of *Calhm2* and microglial conditional knockout of *Calhm2* significantly inhibited two LPS injection–induced decreases in TREM2 levels (fig. 7, K and L). Together, these results suggest that Calhm2 is also involved in LPS-induced neuroinflammation in vivo.

To assess the direct role of Calhm2 in LPS-induced inflammation, we isolated primary microglial from WT mice and *Calhm2* knockout mice. *Calhm2* knockout significantly inhibited LPS-induced increases in IL-1β and TNFα (fig. S8, A and B), suggesting a beneficial role of Calhm2 in LPS-induced inflammatory activation. As there are predicted functions of Calhm2 in NF-κB and mitogen-activated protein kinase (MAPK) signaling, we checked the activation of NF-κB and MAPK signaling in the primary WT microglia and *Calhm2* knockout microglia. As shown in fig. 8 (C to F), *Calhm2* knockout decreased phosphorylated inhibitor of nuclear factor kappa B kinase subunit alpha and beta (p-IKKα/β), phosphorylated c-Jun N-terminal kinase (p-JNK), and phosphorylated extracellular regulated protein kinases 1/2 (p-ERK1/2) levels, suggesting an inhibition of NF-κB and MAPK signaling.

Calhm2 regulates microglial calcium influx and inflammatory activation

Next, we explored how Calhm2 regulates neuroinflammation. As a member of the Calhm genes, we tested whether Calhm2 regulates calcium levels in microglia. We established a consecutive monitoring system and found that *Calhm2* knockout inhibited ATP-induced increases of cytosolic calcium levels (Fig. 6, A and B), suggesting an inhibition of calcium flux. Consistently, phosphorylated calcium/calmodulin-dependent protein kinase II (p-CaMKII) levels were inhibited in *Calhm2* knockout microglia (Fig. 6C and fig. S9A). Moreover, ATP-induced increase of p-CaMKII levels were abolished by treatment with A438079, an inhibitor of P2X7. P2X7, an adenosine receptor that is highly expressed in microglia, plays an important role in AD (*17*, *32*). ATP binds to P2X7 and promotes calcium entry into the cytosolic space and, subsequently, activation of the NLRP3 inflammasome (*33*, *34*). We next checked whether Calhm2 regulates the activity of P2X7 in microglia. As shown in Fig. 6 (D and E), a significant reduction of steady current density, but not the peak current density, was observed in *Calhm2* knockout microglia, suggesting that *Calhm2* knockout mainly affects P2X7 current in microglia (*35*). Given that Cahm2 and P2X7 are both membrane proteins, we then checked whether Calhm2 interacts with P2X7. We found that Calhm2 could bind to P2X7 (fig. S9B) and that *Calhm2* knockout significantly decreased membrane-bound P2X7, with no effect on the total levels of P2X7 in primary microglia in vitro (Fig. 6F and fig. S9C).

It has been reported that P2X7 binds to NLRP3 and acts as an upstream sensor for NLRP3 inflammasome activation, including ATP and Aβ stimulation (*33*, *34*). We then checked whether Calhm2 could influence the interaction between P2X7 and NLRP3. Overexpression of Calhm2 could increase the interaction between P2X7 and NLRP3 (fig. S9D). In addition, we found that P2X7 interacted with the NAIP, CIITA, HET-E, and TP1 (NACHT) and leucine-rich repeat (LRR) domains of NLRP3, but not with the the expanded form of PYD is pyrin-domain (PYD) domain (fig. S9E). Furthermore, *Calhm2* knockout significantly decreased ATP-induced NLRP3 inflammasome activation, and this effect was abolished by adding the P2X7 inhibitor, A438079 (Fig. 6G and fig. S9F). However, treatment with A438079 failed to affect IL-1β and TNFα levels (Fig. 6H), suggesting that P2X7 has no effect on NF-κB signaling activation. Moreover, we found that P2X7 levels were increased in AD mice and that knockout of *Calhm2* inhibited this increase (Fig. 6, I and J). We found that microglial deletion of *Calhm2* reduced P2X7-positive microglia around Aβ plaques (fig. S9, G and H). Furthermore, conventional knockout *Calhm2* or conditional microglial knockout of *Calhm2* both decreased NLRP3 inflammasome activation in AD mice (Fig. 6, K and L, and fig. S9, I and J), suggesting a beneficial role of Calhm2 in the regulation of NLRP3 inflammasome activation. The combined effects of Calhm2 on P2X7 membrane localization and downstream activation of the NLRP3 inflammasome further demonstrated the role of Calhm2 in regulation of inflammatory activation.

In summary, our present work showed that microglial Calhm2 regulates inflammatory activation and contributes to the development of AD and LPS-induced neuroinflammation, in which calcium influx, NF-κB signaling, P2X7 membrane localization, and NLRP3 inflammasome activation are mutually involved in AD-associated microglial dysfunction, presenting a potential therapeutic target for neuroinflammation-related diseases (Fig. 6M).

DISCUSSION

As one of the most common neurodegenerative diseases, AD has been studied for more than 100 years. Although multiple pathological theories have been raised, the underlying mechanism is still unclear, leading to few successful treatments to date. As the predominant

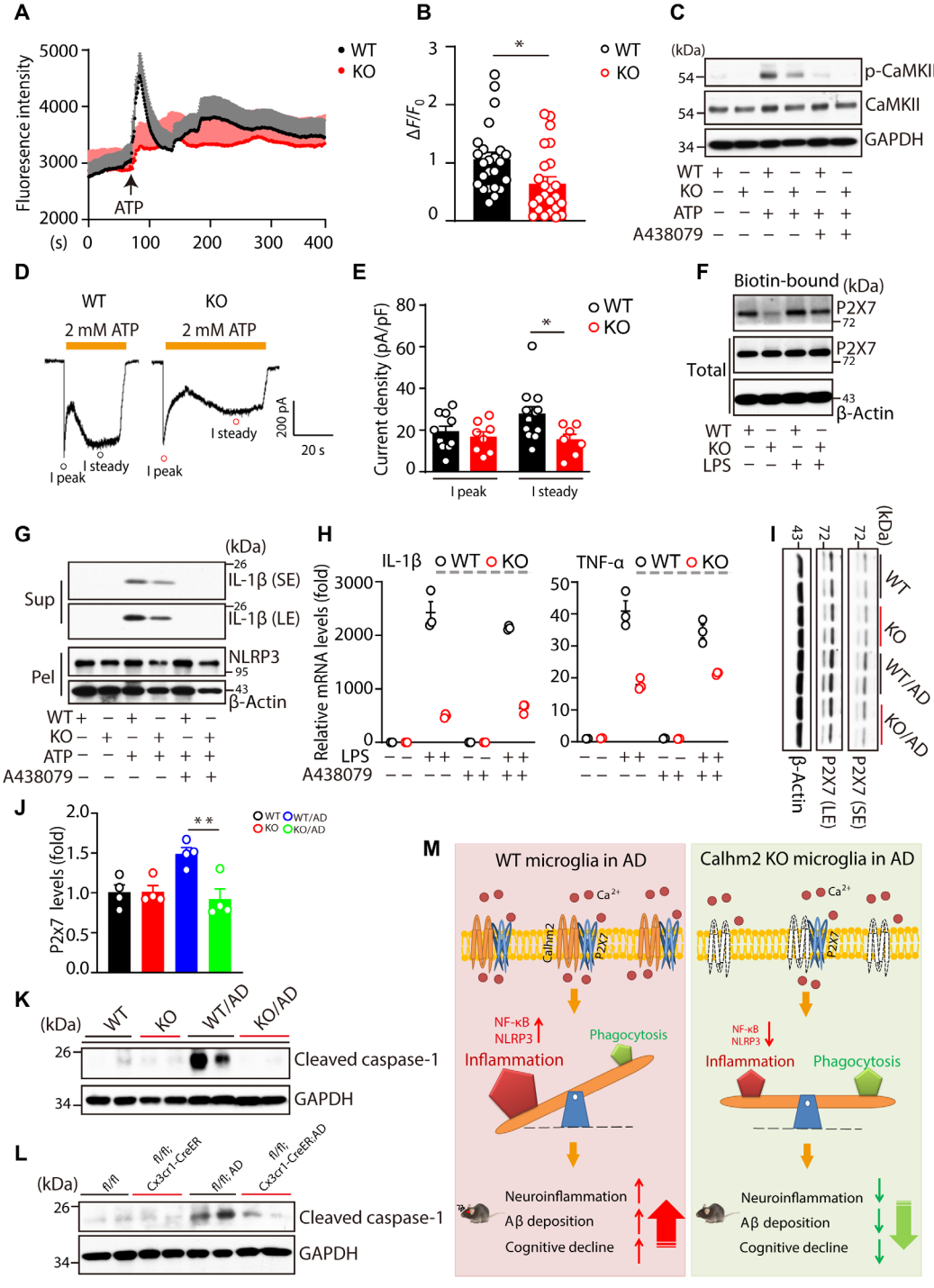

Fig. 6. Calhm2 regulates microglial calcium influx and inflammatory activation. (**A** and **B**) The fluorescence intensity and statistical analysis of fluorescence change ($\Delta F/F_0$) in WT and Calhm2 knockout microglia cells stimulated with 1 mM ATP in the detecting buffer with 2 mM $CaCl_2$. (**C**) Immunoblotting of phosphorylated CaMKII (p-CaMKII) and total CaMKII levels in LPS-primed WT and Calhm2 knockout primary microglia in response to the stimulations induced by ATP and A438079. (**D** and **E**) Representative images and statistical analysis of peak and steady current density (pA/pF) of WT and Calhm2 knockout primary microglia in response to ATP stimulation. The peak current consisted of the response of both P2X4 and P2X7 receptors. Meanwhile, the steady current was the response of only P2X7 receptor. (**F**) Immunoblotting of P2X7 levels in biotin-bound membrane protein. (**G**) Immunoblotting analysis of IL-1β levels in the supernatants of LPS primed WT and Calhm2 knockout primary microglia in response to the stimulations with ATP and A438079. (**H**) Transcriptional levels of IL-1β and TNF-α of WT and Calhm2 knockout primary microglia after LPS stimulation and A438079 treatment. (**I** and **J**) Immunoblotting and quantification of P2X7 levels in 6-month-old WT, *Calhm2*$^{-/-}$, *5×FAD*, and *Calhm2*$^{-/-}$*:5×FAD* mice. One-way ANOVA for multiple groups was based on mouse number. (**K**) Immunoblotting analysis of cleaved caspase-1 in hippocampal tissue of 6-month-old WT, *Calhm2*$^{-/-}$, *5×FAD*, and *Calhm2*$^{-/-}$*:5×FAD* mice. (**L**) Immunoblotting analysis of cleaved caspase-1 in hippocampal tissue of 6-month-old *Calhm2*$^{flox/flox}$, *Calhm2*$^{flox/flox:Cx3cr1\text{-}CreER}$, *Calhm2*$^{flox/flox}$*:5×FAD*, and *Calhm2*$^{flox/flox:Cx3cr1\text{-}CreER}$*:5×FAD* mice. (**M**) The working model of microglial Calhm2 in AD mouse model. *$P < 0.05$ and **$P < 0.01$.

immune cells, microglia are critical to the pathophysiology of AD via the secretion of inflammatory cytokines and direct phagocytosis of Aβ (*36*, *37*). In this study, we found that Calhm2 levels increased in AD brains. By using a well-characterized *5×FAD* mouse model and crossing it with conventional *Calhm2* knockout mice, neuronal *Calhm2* knockout mice, and microglial *Calhm2* knockout mice, we found that conventional deletion of *Calhm2* and conditional deletion of microglial *Calhm2* both significantly decreased Aβ deposition/plaque formation and glial activation and led to significant improvement in the cognitive impairments. Therefore, our results strongly support the role of Calhm2-mediated microglial activation in the progression of AD.

Mechanistically, knockout of *Calhm2* largely inhibited innate immunity signaling genes, especially NF-κB and MAPK signaling. Furthermore, we demonstrated that knockout of *Calhm2* inhibited microglial immune response and inflammatory cytokines levels in vivo and in vitro, suggesting that Calhm2 positively regulates microglial activation. Taking IL-1β as an example, this inflammatory cytokine could suppress microglial phagocytosis of Aβ (*6*, *27*). Here, we found that IL-1β levels increased in AD mice; however, knockout of *Calhm2* decreased IL-1β levels in both isolated microglia and the brain of AD mice. Moreover, knockout of *Calhm2* increased microglial phagocytic activity of Aβ. Further, microglial RNA-seq data and bioinformatic analysis showed that *Calhm2* deficiency also reduced inflammatory activation levels but enhanced protein ubiquitination and proteolysis pathways. We found that microglial *Calhm2* deficiency increased TREM2 levels in primary microglia in vitro and TREM2 immunostaining signals in Aβ plaques surrounding microglia in the brain. TREM2 has an important role in AD development, which is demonstrated to be an Aβ receptor (*5*). TREM2-DNAX activating protein of 12 kDa (DAP12) signaling facilitates microglial phagocytosis and suppresses neuroinflammation. Moreover, the mutations or different cleavage forms of TREM2 make its role more complicated (*38*–*40*). Previous studies show that TREM2 signaling antagonizes Toll-like receptor (TLR) expression and downstream inflammatory cytokine levels mediated by NF-κB signaling. Meanwhile, activation of TLR signaling by LPS stimulation decreases TREM2 expression (*41*, *42*). Moreover, miR-34a, an NF-κB signaling–sensitive microRNA that is highly expressed in patients with AD, has been shown to regulate TREM2 expression in a post-transcriptional manner (*43*). These results suggest that there is a balance between NF-κB signaling activation and TREM2-mediated phagocytic activity. *Calhm2* knockout inhibited microglial proinflammatory activation but increased phagocytic activity, leading to restoration of the balance between inflammation and phagocytosis in AD.

In the CNS, multiple lines of research have shown that calcium dysfunction, especially in neurons, is closely associated with the development of AD, thus raising a calcium-centered hypothesis for AD (*44*, *45*). Involvement of multiple types of calcium channels in AD have been reported, including voltage-operated calcium channels, store-operated calcium channels, neurotransmitter receptors, and Calhm1 (*46*–*48*). Moreover, genetic knockout of calcium channels and specific pharmacological inhibition have protective roles in AD pathology and even in the cognitive function in AD models (*46*, *47*). However, this knowledge does not rule out the role of microglia in this process. Moreover, until now, the role of calcium signaling in microglia in the context of AD has been largely unknown. In vitro experiments show that stimulation of Aβ can increase intracellular calcium levels and induce the activation of the NLRP3 inflammasome in microglia (*17*). Furthermore, the calcium channel blocker, nicardipine, could significantly inhibit LPS/IFN-γ–induced microglial activation (*19*). Activated microglia and increased inflammatory cytokines are observed in the brain of patients with AD. Recently, impairments in calcium homeostasis has been observed in cultured microglia from patients with AD (*49*), implicating a relationship between calcium signaling and microglial activation. In this study, we found that Calhm2 increased in AD mice, consistent with the increase in human Calhm2 from patients with AD. Conditional knockout *Calhm2* in microglia significantly decreased Aβ deposition/plaque formation and cognitive impairment. Together, we have identified Calhm2 as a calcium channel in microglia that plays an important role in the progress of AD in a mouse model. This adds to the literature and provides a deeper understanding of the mechanism underlying microglial activation, suggesting a potential therapeutic candidate for AD treatment.

To better characterize the role of Calhm2 in microglia, in addition to using an AD mouse model, we also used an acute LPS-induced inflammatory model, finding that conventional knockout of *Calhm2* markedly decreased inflammatory cytokines levels and prevented microglial morphological changes. In addition, conditional knockout of *Calhm2* in microglia also significantly inhibited these changes, but with less marked effects compared with the conventional knockout. Moreover, the direct role of Calhm2 in microglia was confirmed in vitro using primary microglia culture. Together, these results demonstrate that Calhm2 is also involved in LPS-induced acute inflammatory activation. Moreover, we argue that apart from microglia, Calhm2 might also function in peripheral immune cells in related diseases, such as sepsis and bacterial infections, warranting further investigation. Recently, the protein structure of human Calhm2 has been identified (*50*, *51*), which could be beneficial for the understanding of the functions of Calhm2 and designing a drug screening system.

The NLRP3 inflammasome is well characterized in AD. *NLRP3* knockout or a dysfunction of its key signaling components significantly reduces Aβ-induced microglial activation in vitro (*52*), decreases Aβ deposition or Tau pathology, and alleviates cognitive impairment in AD mouse models (*6*, *7*). Here, we found that *Calhm2* knockout also significantly decreased NLRP3 inflammasome activation. Mechanistically, we found that Calhm2 not only regulates the transcriptional levels of IL-1β via NF-κB signaling but also functions in the interaction between P2X7 and NLRP3. P2X7 acts as a cation channel that is highly expressed on microglia, which interacts with NLRP3 and regulates its activation (*17*, *32*, *33*). Inhibition of P2X7 decreases microglial inflammatory activation and increases phagocytic activity upon Aβ stimulation in vitro (*53*). Moreover, P2X7 deficiency, induced by genetic deletion or pharmaceutical inhibition, also presents a beneficial role in AD (*54*, *55*). Here, we found that knockout of *Calhm2* decreased the membrane-bound P2X7 on microglia, density currents, and interaction with NLRP3, suggesting an important role of Calhm2 in regulating P2X7 in the microglia. However, some interesting questions remain: (i) Why is Calhm2 increased in activated microglia? Our preliminary data show that Aβ stimulation could induce an increase in the transcriptional levels of Calhm2 in microglia. However, the downstream signaling pathway needs to be investigated. (ii) How does Calhm2 regulate P2X7 membrane localization? P2X7 acts as a protein trafficking molecule between the endoplasmic reticulum and the cell surface (*56*). Until now, what regulates the P2X7 trafficking

mechanism remains unknown. In our RNA-seq data analysis, knockout of *Calhm2* also inhibited vesicle formation and transport, suggesting that vesicle processes might be involved in this mechanism.

Together, in this study, we demonstrated that microglial Calhm2 is not only involved in chronic inflammatory diseases, such as AD, but also has a role in acute inflammatory reactions, suggesting an important role in microglial activation and providing a potential therapeutic target for diseases related to microglia-mediated neuroinflammation.

MATERIALS AND METHODS

Human brain tissue

The human brain tissue was provided by National Human Brain Bank for Development and Function, Chinese Academy of Medical Sciences and Peking Union Medical College, Beijing, China. The information of human brain samples of control and patients with AD were included in table S1.

Mice

Calhm2$^{-/-}$ mice and *Calhm2*$^{flox/flox}$ mice were generated as described in our previous studies. The *5×FAD* mice expressing five familial AD gene mutations have been described (*16*) and were provided by C. Zhang (Peking University, Beijing, China). *Cx3cr1-CreER* mice (purchased from the Jackson laboratory) and *CamKIIα-iCre* mice (*57*) were crossed with *Calhm2*$^{flox/flox}$ mice, respectively. Mice were maintained in the Animal Care Facility at our institute, under ambient temperatures (26° ± 1°C), with a 12-hour light/12-hour dark cycle with unlimited access to standard rodent chow and clean water. All animal experiments were approved by the Institutional Animal Care and Use Committee at Beijing Institute of Basic Medical Sciences.

Tamoxifen (Sigma-Aldrich, catalog no. T5648) was dissolved in corn oil (Sigma-Aldrich, catalog no. C8267). Mice were administrated a total dose of 20 mg of intragastric tamoxifen for three consecutive days.

RNA ISH

ISH experiments were performed in 6-month-old WT and AD mouse brain sections (15 μm) according to the manufacturer's protocol (Advanced Cell Diagnostics).

MWM test

Learning and memory were measured using the MWM test as previously reported but with some modifications (*15*). For the visible platform test, mice were trained in two trials per day for 4 days, with visible platform tagged by a flag in the water maze (22°C) and tested at day 5. For the invisible platform test, mice were trained three times per day for 6 days with the platform hidden, spatial cues presented, and different starting locations for each trial. The average latency to reach the platform was recorded for each trial. On day 7, the platform was removed, and the time spent to cross the platform for the first time, quarter preference, cross platform number, and velocity were recorded.

Open-field test

Mice were subjected to the open-field tests for three consecutive days. Briefly, mice were placed in a quiet and dimly lit environment, and spontaneous activity was monitored for a 5-min period in the apparatus (50 cm × 50 cm × 20 cm). The movements of the mice were analyzed by ANY-maze software.

Microglia isolation from mice brain

Microglial isolation from adult brains was performed as our recent study with some modifications (*58*). Briefly, 6-month-old mice were anesthetized by pentobarbital sodium (70 mg/kg, dissolved in saline) via intraperitoneal injection and perfused transcardially with saline. Whole brain tissue was freshly harvested, cut into small pieces, suspended in Dounce buffer [1.5 mM Hepes and 0.5% glucose in Hanks' balanced salt solution (HBSS) buffer], and homogenized gently using a Dounce homogenizer. Brain tissue homogenates were suspended in phosphate-buffered saline [PBS; NaCl (8 g/liter), KCl (0.2 g/liter), Na_2HPO_4 (1.44 g/liter), and KH_2PO_4 (0.24 g/liter)], filtered with cell strainers (70 μm), and centrifuged at 600*g* for 6 min (4°C) to collect the cell pellets. Then, 100% Percoll solution was prepared with absolute Percoll (GE Healthcare), dissolved in 10× PBS (9:1), and further diluted (v/v) to 70, 37, and 30% with PBS. Cell pellets were suspended in a 37% Percoll solution. Microglia were isolated by density gradient centrifugation. Density gradient was added into 15-ml centrifuge tubes, by layers of Percoll solution from bottom to top containing: 70%, 37% (with cell suspension), and 30% Percoll solution and PBS. Centrifugation was carried out in a horizontal centrifuge at 2000*g* for 30 min (4°C). Microglia were converged on the interphase between the 37 and 70% Percoll solution. Isolated microglia were washed with 10× volumes of PBS and centrifuged at 600*g* for 6 min (4°C). Microglia was further purified by CD11b MicroBeads (Miltenyi Biotec, 130-093-634) according to the manufacturer's protocol.

RNA-seq and bioinformatics analysis

Six mice were chosen from each group. Isolated microglial cells from every three mice were mixed to one sample, after which the RNA extraction and purification were performed. Aliquots of mRNA from three mice in each group were extracted and purified by the NucleoSpin RNA Plus XS Kit (Macherey-Nagel). Libraries were constructed using the Smart-Seq^2 method as previously described (*59*) and sequenced with 10-G depth and paired-end reads on an Illumina HiSeq platform for PE150, performed by Annoroad Gene Technology (Beijing, P. R. China; www.annoroad.com).

Differentially expressed genes ($\log_2$ fold change > 0.5, adjusted false discovery rate < 0.05) between two groups were analyzed using DESeq2 v1.28.1. Since all mice used in this study were male, there was no requirement to adjust the *P* value according to sex when differentially expressed genes were identified. Enriched pathway analysis for differentially expressed genes was conducted by KOBAS 3.0. The rich factor was calculated by dividing the number of differentially expressed genes by the number of all genes in this GO category. GSEA was performed using GSEA v2.0.14 software (www.broadinstitute.org/gsea/index.jsp). Heatmap representation of gene expression was generated by the "pheatmap" package of R (https://CRAN.R-project.org/package=pheatmap).

Acute LPS injection

LPS (0.5 mg/kg; Millipore) administration was done via intraperitoneal injections according to the procedure previously described (*31*). Briefly, mice were treated with a single or double dose of LPS. Each injection was separated by 24 hours. Saline was injected to the control groups. Whole brains were collected

3 hours after the final injection for immunofluorescence experiments, and hippocampal and cortical tissue were collected for qPCR experiments.

Calcium level detection

Primary microglial cells (2×10^5) were cultured in a glass-bottom petri dish overnight. Fluo-4 acetoxymethyl ester (5 ng/μl; Thermo Fisher Scientific) was added into medium and incubated at 37°C for 30 min, followed by washing (×2) with wash buffer [20 mM Hepes (pH 7.4), 0.5 mM $MgCl_2$, 0.4 mM $MgSO_4$, and 5 mM glucose in 1× HBSS]. The cells were incubated with culture medium at 37°C for 30 min. The dish was affixed on a Leica confocal microscope, and the medium was changed. Excitation was performed at 488 nm. The average intensity of the 1-min recording was defined as F_0. The buffer was replaced with an experimental buffer (1 mM ATP). The peak of the 6-min recording was defined as F. Last, calcium activity was calculated as $\Delta F/F_0$, in which $\Delta F = F - F_0$.

Electrophysiology assay

Whole-cell patch-clamp recordings of microglial cells were performed at room temperature using an Axopatch 200B amplifier (Molecular Devices). Current signals were sampled at 10 kHz, filtered at 2 kHz, and analyzed by pClamp 10 (Molecular Devices). Pipettes (resistance ranged from 7 to 10 megohm) were filled with intracellular solution containing 120 mM KCl, 30 mM NaCl, 0.5 mM $CaCl_2$, 2 mM Mg-ATP, 10 mM Hepes, and 5 mM EGTA (pH 7.2). The extracellular recording solution comprised 150 mM NaCl, 5 mM KCl, 10 mM glucose, 10 mM Hepes, 2 mM $CaCl_2$, and 1 mM $MgCl_2$ (pH 7.4). Voltage-dependent current was evoked by pulses from −170 to +30 mV with a 20-mV increment at a holding potential of −70 mV. The holding potential of gap-free recording was −70 mV. ATP and A740003 were dissolved in extracellular recording solution (without Ca^{2+}) and applied using a Y tube.

Primary microglial cell preparation and stimulation

Primary microglial cells were prepared from neonatal mice (ages 1 to 3 days old) as previously described (*14*). Before cell stimulation, 2×10^5 cells were collected and plated into 12-well plates and cultured overnight. Medium was changed to opti-MEM (Thermo Fisher Scientific, catalog no. 31985070) before cell stimulation. For the transcriptional assessments of IL-1β and TNF-α, microglia were stimulated with LPS (1 μg/ml) for 12 or 24 hours. For the analysis of NF-κB signaling activation, the microglia cells were stimulated with LPS (1 μg/ml) for 0.5 or 1 hour. For the assessment of NLRP3 inflammasome activation, microglia cells were primed with LPS (1 μg/ml) for 6 hours, followed by ATP treatment for 30 min. A438079 (a selective antagonist of the P2X7 receptor) was added into the medium 1 hour before the ATP stimulation.

Phagocytosis assays

The phagocytosis assays were performed as previously described (*16*). Briefly, primary microglial cells were plated into 24-well plates and cultured overnight. A final concentration of 1 μg/ml of aggregated FITC-$A\beta_{1-42}$ (AnaSpec, AS-60479) was added to the medium and treated for an indicated time at 37°C. After washing twice with prewarmed PBS, microglial cells were fixed in 4% paraformaldehyde (w/v) for 30 min at room temperature, then washed three times with PBS, and blocked with 10% goat serum (Abcam, catalog no. ab7481) in PBS containing 0.2% Triton X-100 (Sigma-Aldrich, catalog no. V900502). Then, cells were incubated with Iba1 antibody (1:500; WAKO, catalog no. NCNP24) overnight at 4°C. Alexa Fluor 546–conjugated secondary antibody (1:500; Invitrogen, catalog no. A10040) was added for 1 hour at room temperature. Moreover, the phagocytosis assays were confirmed by adding sure aggregated $A\beta_{1-42}$ (AnaSpec, AS-60479) for indicated time at 37°C, and then the supernatant and pellet Aβ were measured by Western Blotting.

Immunohistochemistry and immunofluorescence

All procedures were performed as our previously described studies (*15*). Briefly, mice were perfused with saline, and brains were fixed with 4% paraformaldehyde (w/v) for 1 week. Fixed mouse brains were cryoprotected in 30% sucrose. Coronal sections were cut, and sections were stained with GFAP (1:1000; Sigma-Aldrich, catalog no. G3893), Iba1 (1:500; WAKO, catalog no. NCNP24), CD68 (1:500; Abcam, catalog no. ab53444), TREM2 (1:50; R&D Systems, catalog no. AF1729), and Aβ (1:500; Covance, catalog no. SIG-39320).

The quantification of immunohistochemistry (IHC) was analyzed by the software of Image-Pro Plus (Media Cybernetics Inc.). For quantification of *Calhm2* ISH levels, the spot number of *Calhm2* staining in each cell was counted in the indicated brain area. For Iba1 or GFAP IHC levels, we have counted all the intact cells from same pixel area in the indicated brain area.

Microglial skeleton analysis

The skeleton analysis of microglia was performed as previously described (*60*). Briefly, the images were captured in 20 μm using a Z-series stack of Nikon A1 confocal microscope. Skeletonize [two-dimensional (2D)/3D] plugin of the software ImageJ (National Institutes of Health, USA) was used for the skeleton analysis, and AnalyzeSkeleton plugin was used for the length and process number analysis.

Biotinylation of microglial cell surface P2X7

Biotinylation of surface P2X7 assay was performed as described previously but with slight modification (*61*). Briefly, primary WT or *Calhm2* KO microglia were seeded in a 6-cm cell plate followed by stimulation with LPS (1 μg/ml) for 6 hours. Then, the cells were washed three times with ice-cold Dulbecco's phosphate-buffered saline (DPBS) ($CaCl_2$ and $MgCl_2$ free) and incubated with freshly prepared Sulfo-NHS-SS-biotin (1 mg/ml, diluted in DPBS; Pierce, catalog no. 21331) for 30 min at 12°C. Nonreactive biotin was quenched with 50 mM glycine followed by three washes with cold DPBS to remove unbound biotin. The cells were subsequently lysed with 500 μl of cell lysis buffer [50 mM tris (pH 7.4), 150 mM NaCl, 1 mM EDTA, 1% Triton X-100, 1% sodium deoxycholate, and 0.1% SDS] followed by sonication to further disrupt and homogenize the cells. The resultant lysate was cleared by centrifugation at 14,000 rpm for 15 min at 4°C. The biotinylated P2X7 in the supernatant was precipitated by incubation with 30 μl of streptavidin beads (Pierce, catalog no. 88816) on a rotating wheel at 4°C for 2 hours followed by four washes with cell lysis buffer. The biotinylated P2X7 bound to streptavidin beads was eluted with 1× SDS loading buffer and analyzed by Western blotting.

Immunoprecipitation and immunoblot analysis

Coimmunoprecipitation and immunoblotting were performed as described previously (*14*). Human embryonic kidney (HEK) 293T cells were plated into a six-well plate and cultured overnight. The plamids

were transfected into HEK293T cells as indicated. Twenty-four hours later, coimmunoprecipitation and immunoblotting analysis were performed. Samples were fractionated by SDS–polyacrylamide gel electrophoresis and transferred to nitrocellulose membranes (GE Amersham, catalog no. 10600002). Immunoblots were probed with the primary antibodies (as shown in table S2) and visualized by enhanced chemiluminescence (Thermo Fisher Scientific, catalog no. 32106).

Enzyme-linked immunosorbent assay

Levels of $A\beta_{1-40}$ and $A\beta_{1-42}$ in soluble or insoluble mouse brain hippocampal tissue extractions were measured as described before (*16*), according to the manufacturer's instructions (R&D Systems, Minneapolis, MN, USA).

Quantitative RT-PCR

Total RNA was extracted from brain samples or cell samples using TRIzol reagent (Invitrogen, catalog no. 15596018). One microgram of RNA was used in a one-step first-strand cDNA synthesis kit (TransGen Biotech, catalog no. AT341). Quantitative real-time (RT) PCR was performed using 2× SYBR Green PCR master mix (TransGen Biotech, catalog no. AQ131) and an Agilent Mx3005P RT-PCR system. The primers used for analysis are listed in table S2. The mRNA levels of tested genes were normalized to *Gapdh* expression levels.

Statistical analysis

Statistical analysis was performed using Student's *t* tests for comparisons between two groups, and one-way analysis of variance (ANOVA) was performed for multiple groups using GraphPad (Prism GraphPad software). All values are expressed as the means ± SEM. P values < 0.05 were considered significant.

SUPPLEMENTARY MATERIALS

Supplementary material for this article is available at http://advances.sciencemag.org/cgi/content/full/7/35/eabe3600/DC1

View/request a protocol for this paper from *Bio-protocol*.

REFERENCES AND NOTES

1. M. B. Graeber, S. Kosel, R. Egensperger, R. B. Banati, U. Muller, K. Bise, P. Hoff, H. J. Moller, K. Fujisawa, P. Mehraein, Rediscovery of the case described by Alois Alzheimer in 1911: Historical, histological and molecular genetic analysis. *Neurogenetics* **1**, 73–80 (1997).
2. A. Verkhratsky, R. Zorec, J. J. Rodriguez, V. Parpura, Astroglia dynamics in ageing and Alzheimer's disease. *Curr. Opin. Pharmacol.* **26**, 74–79 (2016).
3. C. M. Karch, A. M. Goate, Alzheimer's disease risk genes and mechanisms of disease pathogenesis. *Biol. Psychiatry* **77**, 43–51 (2015).
4. T. K. Ulland, W. M. Song, S. C. Huang, J. D. Ulrich, A. Sergushichev, W. L. Beatty, A. A. Loboda, Y. Zhou, N. J. Cairns, A. Kambal, E. Loginicheva, S. Gilfillan, M. Cella, H. W. Virgin, E. R. Unanue, Y. Wang, M. N. Artyomov, D. M. Holtzman, M. Colonna, TREM2 maintains microglial metabolic fitness in Alzheimer's disease. *Cell* **170**, 649–663.e13 (2017).
5. Y. Zhao, X. Wu, X. Li, L.-L. Jiang, X. Gui, Y. Liu, Y. Sun, B. Zhu, J. C. Piña-Crespo, M. Zhang, N. Zhang, X. Chen, G. Bu, Z. An, T. Y. Huang, H. Xu, TREM2 is a receptor for β-amyloid that mediates microglial function. *Neuron* **97**, 1023–1031.e7 (2018).
6. M. T. Heneka, M. P. Kummer, A. Stutz, A. Delekate, S. Schwartz, A. Vieira-Saecker, A. Griep, D. Axt, A. Remus, T. C. Tzeng, E. Gelpi, A. Halle, M. Korte, E. Latz, D. T. Golenbock, NLRP3 is activated in Alzheimer's disease and contributes to pathology in APP/PS1 mice. *Nature* **493**, 674–678 (2013).
7. C. Ising, C. Venegas, S. Zhang, H. Scheiblich, S. V. Schmidt, A. Vieira-Saecker, S. Schwartz, S. Albasset, R. M. McManus, D. Tejera, A. Griep, F. Santarelli, F. Brosseron, S. Opitz, J. Stunden, M. Merten, R. Kayed, D. T. Golenbock, D. Blum, E. Latz, L. Buee, M. T. Heneka, NLRP3 inflammasome activation drives tau pathology. *Nature* **575**, 669–673 (2019).
8. C. Venegas, S. Kumar, B. S. Franklin, T. Dierkes, R. Brinkschulte, D. Tejera, A. Vieira-Saecker, S. Schwartz, F. Santarelli, M. P. Kummer, A. Griep, E. Gelpi, M. Beilharz, D. Riedel, D. T. Golenbock, M. Geyer, J. Walter, E. Latz, M. T. Heneka, Microglia-derived ASC specks cross-seed amyloid-β in Alzheimer's disease. *Nature* **552**, 355–361 (2017).
9. A. Griciuc, S. Patel, A. N. Federico, S. H. Choi, B. J. Innes, M. K. Oram, G. Cereghetti, D. McGinty, A. Anselmo, R. I. Sadreyev, S. E. Hickman, J. El Khoury, M. Colonna, R. E. Tanzi, TREM2 acts downstream of CD33 in modulating microglial pathology in Alzheimer's disease. *Neuron* **103**, 820–835.e7 (2019).
10. J. V. Pluvinage, M. S. Haney, B. A. H. Smith, J. Sun, T. Iram, L. Bonanno, L. Li, D. P. Lee, D. W. Morgens, A. C. Yang, S. R. Shuken, D. Gate, M. Scott, P. Khatri, J. Luo, C. R. Bertozzi, M. C. Bassik, T. Wyss-Coray, CD22 blockade restores homeostatic microglial phagocytosis in ageing brains. *Nature* **568**, 187–192 (2019).
11. B. Korin, T. L. Ben-Shaanan, M. Schiller, T. Dubovik, H. Azulay-Debby, N. T. Boshnak, T. Koren, A. Rolls, High-dimensional, single-cell characterization of the brain's immune compartment. *Nat. Neurosci.* **20**, 1300–1309 (2017).
12. F. Ginhoux, M. Prinz, Origin of microglia: Current concepts and past controversies. *Cold Spring Harb. Perspect. Biol.* **7**, a020537 (2015).
13. H. Keren-Shaul, A. Spinrad, A. Weiner, O. Matcovitch-Natan, R. Dvir-Szternfeld, T. K. Ulland, E. David, K. Baruch, D. Lara-Astaiso, B. Toth, S. Itzkovitz, M. Colonna, M. Schwartz, I. Amit, A unique microglia type associated with restricting development of Alzheimer's disease. *Cell* **169**, 1276–1290.e17 (2017).
14. J. Cheng, Y. Liao, L. Xiao, R. Wu, S. Zhao, H. Chen, B. Hou, X. Zhang, C. Liang, Y. Xu, Z. Yuan, Autophagy regulates MAVS signaling activation in a phosphorylation-dependent manner in microglia. *Cell Death Differ.* **24**, 276–287 (2017).
15. J. Cheng, Y. Liao, Y. Dong, H. Hu, N. Yang, X. Kong, S. Li, X. Li, J. Guo, L. Qin, J. Yu, C. Ma, J. Li, M. Li, B. Tang, Z. Yuan, Microglial autophagy defect causes parkinson disease-like symptoms by accelerating inflammasome activation in mice. *Autophagy* **16**, 2193–2205 (2020).
16. R.-Y. Pan, J. Ma, X.-X. Kong, X.-F. Wang, S.-S. Li, X.-L. Qi, Y.-H. Yan, J. Cheng, Q. Liu, W. Jin, C.-H. Tan, Z. Yuan, Sodium rutin ameliorates Alzheimer's disease–like pathology by enhancing microglial amyloid-β clearance. *Sci. Adv.* **5**, eaau6328 (2019).
17. P. Chiozzi, A. C. Sarti, J. M. Sanz, A. L. Giuliani, E. Adinolfi, V. Vultaggio-Poma, S. Falzoni, F. Di Virgilio, Amyloid β-dependent mitochondrial toxicity in mouse microglia requires P2X7 receptor expression and is prevented by nimodipine. *Sci. Rep.* **9**, 6475 (2019).
18. G. S. Lee, N. Subramanian, A. I. Kim, I. Aksentijevich, R. Goldbach-Mansky, D. B. Sacks, R. N. Germain, D. L. Kastner, J. J. Chae, The calcium-sensing receptor regulates the NLRP3 inflammasome through Ca^{2+} and cAMP. *Nature* **492**, 123–127 (2012).
19. B.-R. Huang, P.-C. Chang, W.-L. Yeh, C.-H. Lee, C.-F. Tsai, C. Lin, H.-Y. Lin, Y.-S. Liu, C. Y. Wu, P. Y. Ko, S.-S. Huang, H.-C. Hsu, D.-Y. Lu, Anti-neuroinflammatory effects of the calcium channel blocker nicardipine on microglial cells: Implications for neuroprotection. *PLOS ONE* **9**, e91167 (2014).
20. U. Dreses-Werringloer, J. C. Lambert, V. Vingtdeux, H. Zhao, H. Vais, A. Siebert, A. Jain, J. Koppel, A. Rovelet-Lecrux, D. Hannequin, F. Pasquier, D. Galimberti, E. Scarpini, D. Mann, C. Lendon, D. Campion, P. Amouyel, P. Davies, J. K. Foskett, F. Campagne, P. Marambaud, A polymorphism in CALHM1 influences Ca^{2+} homeostasis, Abeta levels, and Alzheimer's disease risk. *Cell* **133**, 1149–1161 (2008).
21. J. Wu, S. Peng, R. Wu, Y. Hao, G. Ji, Z. Yuan, Generation of Calhm1 knockout mouse and characterization of calhm1 gene expression. *Protein Cell* **3**, 470–480 (2012).
22. A. Taruno, V. Vingtdeux, M. Ohmoto, Z. Ma, G. Dvoryanchikov, A. Li, L. Adrien, H. Zhao, S. Leung, M. Abernethy, J. Koppel, P. Davies, M. M. Civan, N. Chaudhari, I. Matsumoto, G. Hellekant, M. G. Tordoff, P. Marambaud, J. K. Foskett, CALHM1 ion channel mediates purinergic neurotransmission of sweet, bitter and umami tastes. *Nature* **495**, 223–226 (2013).
23. Z. Ma, A. Taruno, M. Ohmoto, M. Jyotaki, J. C. Lim, H. Miyazaki, N. Niisato, Y. Marunaka, R. J. Lee, H. Hoff, R. Payne, A. Demuro, I. Parker, C. H. Mitchell, J. Henao-Mejia, J. E. Tanis, I. Matsumoto, M. G. Tordoff, J. K. Foskett, CALHM3 is essential for rapid ion channel-mediated purinergic neurotransmission of GPCR-mediated tastes. *Neuron* **98**, 547–561.e10 (2018).
24. M. Jun, Q. Xiaolong, Y. Chaojuan, P. Ruiyuan, W. Shukun, W. Junbing, H. Li, C. Hong, C. Jinbo, W. Rong, L. Yajin, M. Lanqun, W. Fengchao, W. Zhiying, A. Jianxiong, W. Yun, Z. Xia, Z. Chen, Y. Zengqiang, Calhm2 governs astrocytic ATP releasing in the development of depression-like behaviors. *Mol. Psychiatry* **23**, 229–238 (2018).
25. M. T. Heneka, M. J. Carson, J. El Khoury, G. E. Landreth, F. Brosseron, D. L. Feinstein, A. H. Jacobs, T. Wyss-Coray, J. Vitorica, R. M. Ransohoff, K. Herrup, S. A. Frautschy, B. Finsen, G. C. Brown, A. Verkhratsky, K. Yamanaka, J. Koistinaho, E. Latz, A. Halle, G. C. Petzold, T. Town, D. Morgan, M. L. Shinohara, V. H. Perry, C. Holmes, N. G. Bazan, D. J. Brooks, S. Hunot, B. Joseph, N. Deigendesch, O. Garaschuk, E. Boddeke, C. A. Dinarello, J. C. Breitner, G. M. Cole, D. T. Golenbock, M. P. Kummer, Neuroinflammation in Alzheimer's disease. *Lancet. Neurol.* **14**, 388–405 (2015).
26. C. N. Parkhurst, G. Yang, I. Ninan, J. N. Savas, J. R. Yates III, J. J. Lafaille, B. L. Hempstead, D. R. Littman, W.-B. Gan, Microglia promote learning-dependent synapse formation through brain-derived neurotrophic factor. *Cell* **155**, 1596–1609 (2013).
27. J. Koenigsknecht-Talboo, G. E. Landreth, Microglial phagocytosis induced by fibrillar β-amyloid and IgGs are differentially regulated by proinflammatory cytokines. *J. Neurosci.* **25**, 8240–8249 (2005).

28. T. Minett, J. Classey, F. E. Matthews, M. Fahrenhold, M. Taga, C. Brayne, P. G. Ince, J. A. Nicoll, D. Boche; MRC CFAS, Microglial immunophenotype in dementia with Alzheimer's pathology. *J. Neuroinflammation* **13**, 135 (2016).
29. A. Deczkowska, A. Weiner, I. Amit, The physiology, pathology, and potential therapeutic applications of the TREM2 signaling pathway. *Cell* **181**, 1207–1217 (2020).
30. L. Zhong, Z. Wang, D. Wang, Z. Wang, Y. A. Martens, L. Wu, Y. Xu, K. Wang, J. Li, R. Huang, D. Can, H. Xu, G. Bu, X.-F. Chen, Amyloid-beta modulates microglial responses by binding to the triggering receptor expressed on myeloid cells 2 (TREM2). *Mol. Neurodegener.* **13**, 15 (2018).
31. A. C. Wendeln, K. Degenhardt, L. Kaurani, M. Gertig, T. Ulas, G. Jain, J. Wagner, L. M. Hasler, K. Wild, A. Skodras, T. Blank, O. Staszewski, M. Datta, T. P. Centeno, V. Capece, M. R. Islam, C. Kerimoglu, M. Staufenbiel, J. L. Schultze, M. Beyer, M. Prinz, M. Jucker, A. Fischer, J. J. Neher, Innate immune memory in the brain shapes neurological disease hallmarks. *Nature* **556**, 332–338 (2018).
32. H. G. Lee, S. M. Won, B. J. Gwag, Y. B. Lee, Microglial $P2X_7$ receptor expression is accompanied by neuronal damage in the cerebral cortex of the APPswe/PS1dE9 mouse model of Alzheimer's disease. *Exp. Mol. Med.* **43**, 7–14 (2011).
33. A. Franceschini, M. Capece, P. Chiozzi, S. Falzoni, J. M. Sanz, A. C. Sarti, M. Bonora, P. Pinton, F. Di Virgilio, The P2X7 receptor directly interacts with the NLRP3 inflammasome scaffold protein. *FASEB J.* **29**, 2450–2461 (2015).
34. M. Karmakar, M. A. Katsnelson, G. R. Dubyak, E. Pearlman, Neutrophil $P2X_7$ receptors mediate NLRP3 inflammasome-dependent IL-1β secretion in response to ATP. *Nat. Commun.* **7**, 10555 (2016).
35. R. Raouf, A. J. Chabot-Dore, A. R. Ase, D. Blais, P. Seguela, Differential regulation of microglial P2X4 and P2X7 ATP receptors following LPS-induced activation. *Neuropharmacology* **53**, 496–504 (2007).
36. M. W. Salter, B. Stevens, Microglia emerge as central players in brain disease. *Nat. Med.* **23**, 1018–1027 (2017).
37. A. Deczkowska, I. Amit, M. Schwartz, Microglial immune checkpoint mechanisms. *Nat. Neurosci.* **21**, 779–786 (2018).
38. M. M. Painter, Y. Atagi, C. C. Liu, R. Rademakers, H. Xu, J. D. Fryer, G. Bu, TREM2 in CNS homeostasis and neurodegenerative disease. *Mol. Neurodegener.* **10**, 43 (2015).
39. H. Zheng, L. Jia, C. C. Liu, Z. Rong, L. Zhong, L. Yang, X. F. Chen, J. D. Fryer, X. Wang, Y. W. Zhang, H. Xu, G. Bu, TREM2 promotes microglial survival by activating Wnt/β-catenin pathway. *J. Neurosci.* **37**, 1772–1784 (2017).
40. L. Zhong, Y. Xu, R. Zhuo, T. Wang, K. Wang, R. Huang, D. Wang, Y. Gao, Y. Zhu, X. Sheng, K. Chen, N. Wang, L. Zhu, D. Can, Y. Marten, M. Shinohara, C. C. Liu, D. Du, H. Sun, L. Wen, H. Xu, G. Bu, X. F. Chen, Soluble TREM2 ameliorates pathological phenotypes by modulating microglial functions in an Alzheimer's disease model. *Nat. Commun.* **10**, 1365 (2019).
41. H. Ito, J. A. Hamerman, TREM-2, triggering receptor expressed on myeloid cell-2, negatively regulates TLR responses in dendritic cells. *Eur. J. Immunol.* **42**, 176–185 (2012).
42. X. Gao, Y. Dong, Z. Liu, B. Niu, Silencing of triggering receptor expressed on myeloid cells-2 enhances the inflammatory responses of alveolar macrophages to lipopolysaccharide. *Mol. Med. Rep.* **7**, 921–926 (2013).
43. Y. Zhao, S. Bhattacharjee, B. M. Jones, P. Dua, P. N. Alexandrov, J. M. Hill, W. J. Lukiw, Regulation of TREM2 expression by an NF-κB-sensitive miRNA-34a. *Neuroreport* **24**, 318–323 (2013).
44. Z. S. Khachaturian, Calcium, membranes, aging, and Alzheimer's disease. Introduction and overview. *Ann. N. Y. Acad. Sci.* **568**, 1–4 (1989).
45. Alzheimer's Association Calcium Hypothesis Workgroup, Calcium hypothesis of Alzheimer's disease and brain aging: A framework for integrating new evidence into a comprehensive theory of pathogenesis. *Alzheimers Dement.* **13**, 178–182.e17 (2017).
46. W. V. Goodison, V. Frisardi, P. G. Kehoe, Calcium channel blockers and Alzheimer's disease: Potential relevance in treatment strategies of metabolic syndrome. *J. Alzheimer's Dis.* **30** (Suppl. 2), S269–S282 (2012).
47. Y. Tan, Y. Deng, H. Qing, Calcium channel blockers and Alzheimer's disease. *Neural Regen. Res.* **7**, 137–140 (2012).
48. A. J. Moreno-Ortega, I. Buendia, L. Mouhid, J. Egea, S. Lucea, A. Ruiz-Nuno, M. G. Lopez, M. F. Cano-Abad, CALHM1 and its polymorphism P86L differentially control Ca^{2+} homeostasis, mitogen-activated protein kinase signaling, and cell vulnerability upon exposure to amyloid β. *Aging Cell* **14**, 1094–1102 (2015).
49. J. G. McLarnon, H. B. Choi, L. F. Lue, D. G. Walker, S. U. Kim, Perturbations in calcium-mediated signal transduction in microglia from Alzheimer's disease patients. *J. Neurosci. Res.* **81**, 426–435 (2005).
50. W. Choi, N. Clemente, W. Sun, J. Du, W. Lu, The structures and gating mechanism of human calcium homeostasis modulator 2. *Nature* **576**, 163–167 (2019).
51. J. L. Syrjanen, K. Michalski, T. H. Chou, T. Grant, S. Rao, N. Simorowski, S. J. Tucker, N. Grigorieff, H. Furukawa, Structure and assembly of calcium homeostasis modulator proteins. *Nat. Struct. Mol. Biol.* **27**, 150–159 (2020).
52. A. Halle, V. Hornung, G. C. Petzold, C. R. Stewart, B. G. Monks, T. Reinheckel, K. A. Fitzgerald, E. Latz, K. J. Moore, D. T. Golenbock, The NALP3 inflammasome is involved in the innate immune response to amyloid-β. *Nat. Immunol.* **9**, 857–865 (2008).
53. J. Ni, P. Wang, J. Zhang, W. Chen, L. Gu, Silencing of the $P2X_7$ receptor enhances amyloid-β phagocytosis by microglia. *Biochem. Biophys. Res. Commun.* **434**, 363–369 (2013).
54. X. Chen, J. Hu, L. Jiang, S. Xu, B. Zheng, C. Wang, J. Zhang, X. Wei, L. Chang, Q. Wang, Brilliant Blue G improves cognition in an animal model of Alzheimer's disease and inhibits amyloid-β-induced loss of filopodia and dendrite spines in hippocampal neurons. *Neuroscience* **279**, 94–101 (2014).
55. E. Martin, M. Amar, C. Dalle, I. Youssef, C. Boucher, C. Le Duigou, M. Bruckner, A. Prigent, V. Sazdovitch, A. Halle, J. M. Kanellopoulos, B. Fontaine, B. Delatour, C. Delarasse, New role of P2X7 receptor in an Alzheimer's disease mouse model. *Mol. Psychiatry* **24**, 108–125 (2019).
56. L. Gudipaty, B. D. Humphreys, G. Buell, G. R. Dubyak, Regulation of $P2X_7$ nucleotide receptor function in human monocytes by extracellular ions and receptor density. *Am. J. Physiol. Cell Physiol.* **280**, C943–C953 (2001).
57. R. Wu, H. Chen, J. Ma, Q. He, Q. Huang, Q. Liu, M. Li, Z. Yuan, c-Abl–p38α signaling plays an important role in MPTP-induced neuronal death. *Cell Death Differ.* **23**, 542–552 (2016).
58. Y. Dong, S. Li, Y. Lu, X. Li, Y. Liao, Z. Peng, Y. Li, L. Hou, Z. Yuan, J. Cheng, Stress-induced NLRP3 inflammasome activation negatively regulates fear memory in mice. *J. Neuroinflammation* **17**, 205 (2020).
59. S. Picelli, O. R. Faridani, A. K. Bjorklund, G. Winberg, S. Sagasser, R. Sandberg, Full-length RNA-seq from single cells using Smart-seq2. *Nat. Protoc.* **9**, 171–181 (2014).
60. S. Li, Y. Liao, Y. Dong, X. Li, J. Li, Y. Cheng, J. Cheng, Z. Yuan, Microglial deletion and inhibition alleviate behavior of post-traumatic stress disorder in mice. *J. Neuroinflammation* **18**, 7 (2021).
61. M. Boumechache, M. Masin, J. M. Edwardson, D. C. Gorecki, R. Murrell-Lagnado, Analysis of assembly and trafficking of native P2X4 and P2X7 receptor complexes in rodent immune cells. *J. Biol. Chem.* **284**, 13446–13454 (2009).

Acknowledgments: We thank C. Zhang (Peking University, Beijing, China) for providing *5×FAD* mice. We acknowledge National Human Brain Bank for Development and Function (Chinese Academy of Medical Sciences and Peking Union Medical College, Beijing, China) for providing the human brain tissue. **Funding:** This work was supported by grants from the National Natural Science Foundation of China (grant nos. 81870839, 82071218, 81630026, and 81930029). This study was also supported by the Institute of Basic Medical Sciences, Chinese Academy of Medical Sciences, Neuroscience Center and the China Human Brain Banking Consortium. **Author contributions:** J.C. designed and performed experiments, analyzed data, and wrote the paper. Y.D., J.M., R.P., Y.L., and X.K. performed some experiments and analyzed data. S.L. and X.L. provided samples or reagents and analyzed data. P.C. and Y.Y. helped for the P2X7 density currency study and advice. L.W. helped with the RNA-seq analysis. Z.Y. supervised this research, analyzed data, and wrote the paper. **Competing interests:** The authors declare that they have no competing interests. **Data and materials availability:** All data needed to evaluate the conclusions in the paper are present in the paper and/or the Supplementary Materials. The differentially expressed genes and enrichment analyses related to gene expression have been provided in supplementary files. In addition, RNA-seq raw data have been deposited at GEO (https://www.ncbi.nlm.nih.gov/geo/) with the number of GSE164415.

Submitted 17 August 2020
Accepted 6 July 2021
Published 25 August 2021
10.1126/sciadv.abe3600

Citation: J. Cheng, Y. Dong, J. Ma, R. Pan, Y. Liao, X. Kong, X. Li, S. Li, P. Chen, L. Wang, Y. Yu, Z. Yuan, Microglial Calhm2 regulates neuroinflammation and contributes to Alzheimer's disease pathology. *Sci. Adv.* **7**, eabe3600 (2021).